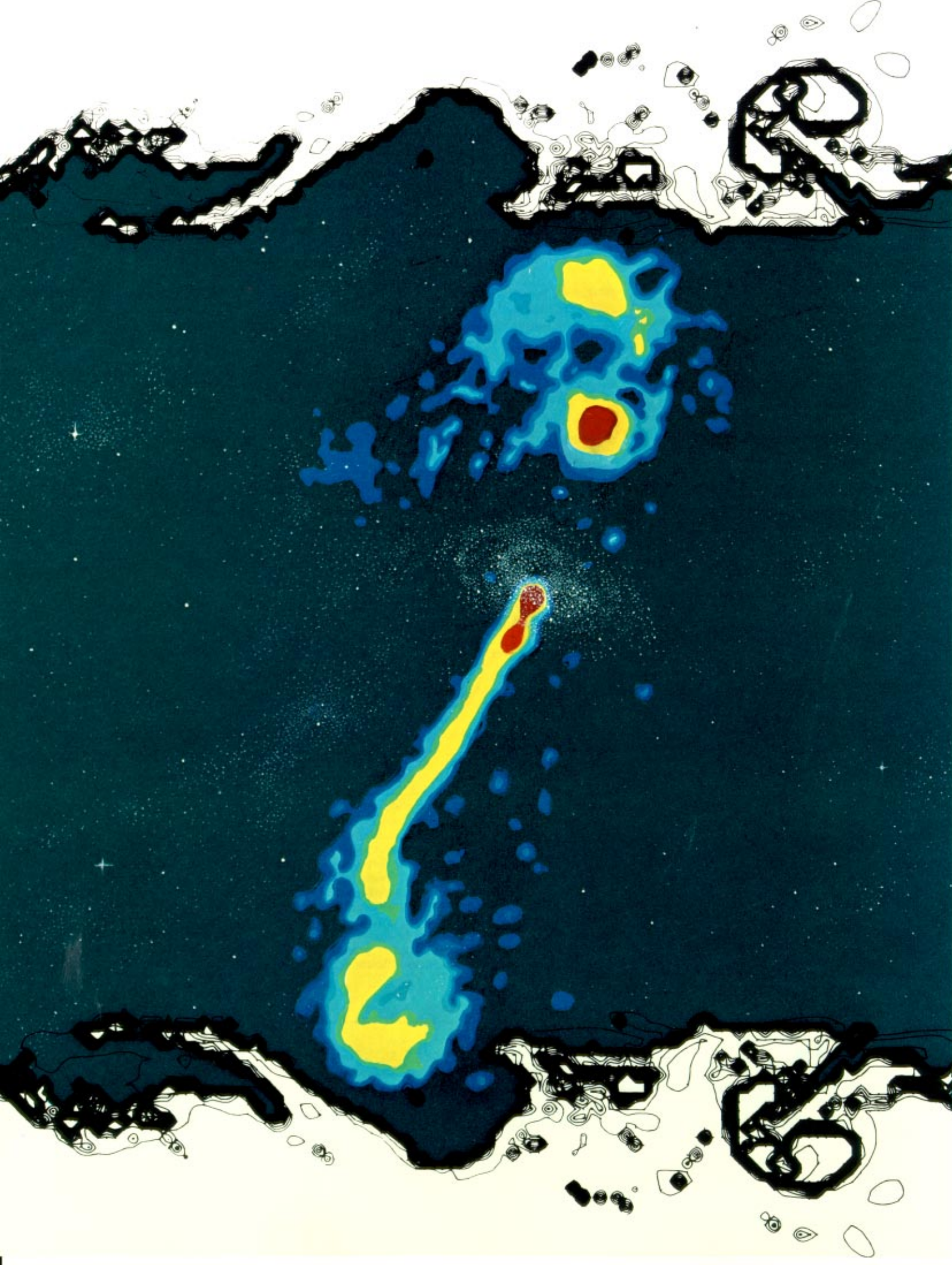

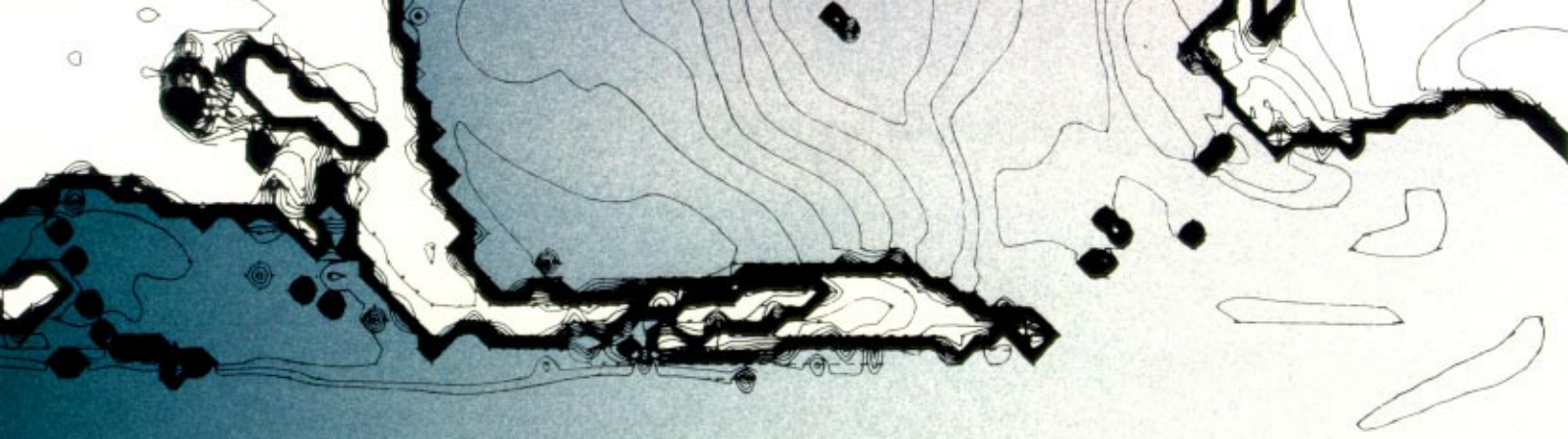

SUPERSONIC JETS

Nonlinear features of supersonic jet flow may explain the mysterious stability of extragalactic jets.

by Michael L. Norman and Karl-Heinz A. Winkler

To the man on the street, a supersonic jet is an aircraft that travels faster than the speed of sound and rattles windows and teacups with its sonic boom. In fact, he is doubly correct. Every aircraft like the Concorde or the F-15 not only *is* a supersonic jet but also creates one of another kind. The gaseous exhaust, which according to Newton's third law propels the aircraft forward, is expelled from the engine supersonically, that is, with a speed well in excess of the speed of sound in the gas. The gas forms a well-collimated jet that remains stable over a distance many times as long as its diameter (Fig. 1). This second type of supersonic jet occurs naturally in many contexts and over many distance scales. Moreover, it exhibits remarkable features of structure and stability that challenge the modeling capabilities of modern numerical hydrodynamicists.

Our interest in supersonic gas jets has been twofold. First, we wanted to exploit the inherent flexibility of numerical modeling to explore supersonic flow over a wider range of physical parameters than has been investigated experimentally. Second, we wondered whether through these simulations we could explain the extraordinary stability of astrophysical jets, which, as shown in the opening illustration, can bore their way through intergalactic space from the center of a radio galaxy to distances of thousands or millions of light years. Could we capture in numerical simulations the coherent nonlinear structures that seem to appear in both astrophysical and terrestrial supersonic jets?

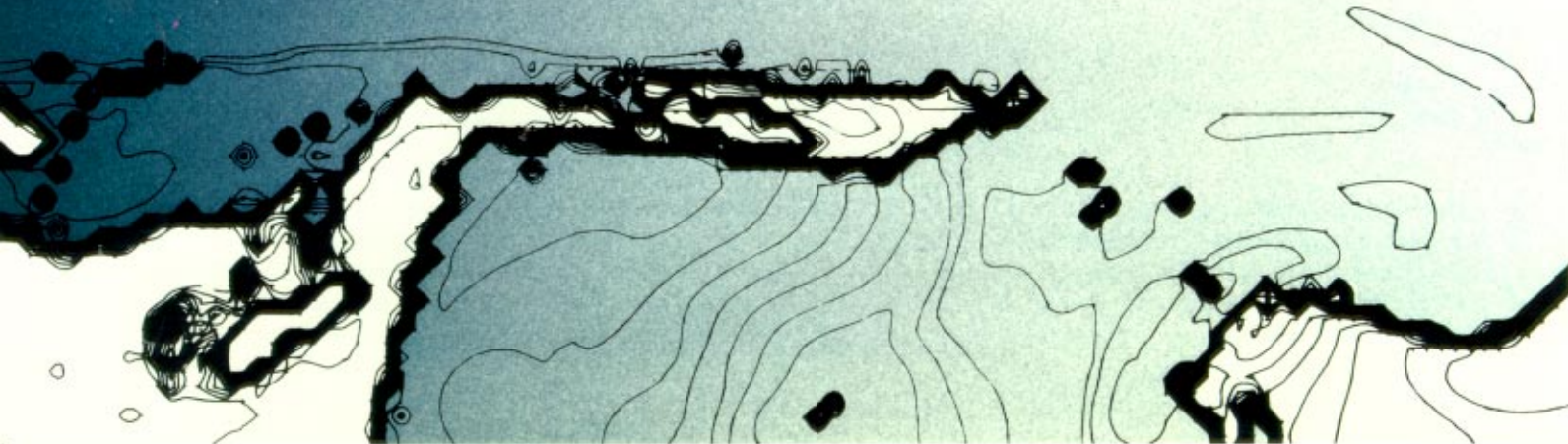

Fig. 1. A supersonic exhaust jet trailing the Bell X-1 rocket plane, the first manned aircraft to break the sound barrier. The beaded appearance of the jet is due to a network of internal shock waves that repeatedly compresses and reheats the exhaust gas. (From "Orders of Magnitude'' by F. W. Anderson, NASA Special Publication 4403, 1981.)

The results we present here were achieved in collaboration with Larry L. Smarr of the University of Illinois and are based solely on numerical simulations carried out on a Cray-1 computer at the Max Planck Institut fur Physik und Astrophysik in Garching bei Munchen. Working in West Germany, we were constantly reminded of the dual definition of a supersonic jet as NATO forces maneuvered overhead. This was strangely appropriate, however, for the history of research on supersonic gas jets goes back nearly a century to the pioneering work of Ernst Mach at the behest of the Austrian military.

Ernst Mach and the Military Connection

Back in the 1880s the concept of a shock wave was still brand new. In Europe the theoretical properties of these nonlinear compression waves were being hotly debated by the likes of Riemann, Rankine, Rayleigh, and Hugoniot. It was still uncertain whether it was energy or entropy that is conserved across the surface of discontinuity created by a shock front (see Sidebar 1, "Shock Waves versus Sound Waves").

Meanwhile, artillery experts and ballisticians were groping for explanations of two curious phenomena brought to light during the France-Prussian War. The first was the double report heard when a shell was fired at high speed from an artillery piece; only a single report was heard when a projectile was fired at low speed. The second was the crater-like nature of the wounds inflicted by the French army's new high-speed bullets. Exploding bullets—expressly forbidden by treaty—were suspected as having been used.

The Belgian ballistician Melsens proposed an explanation for the second phenomenon

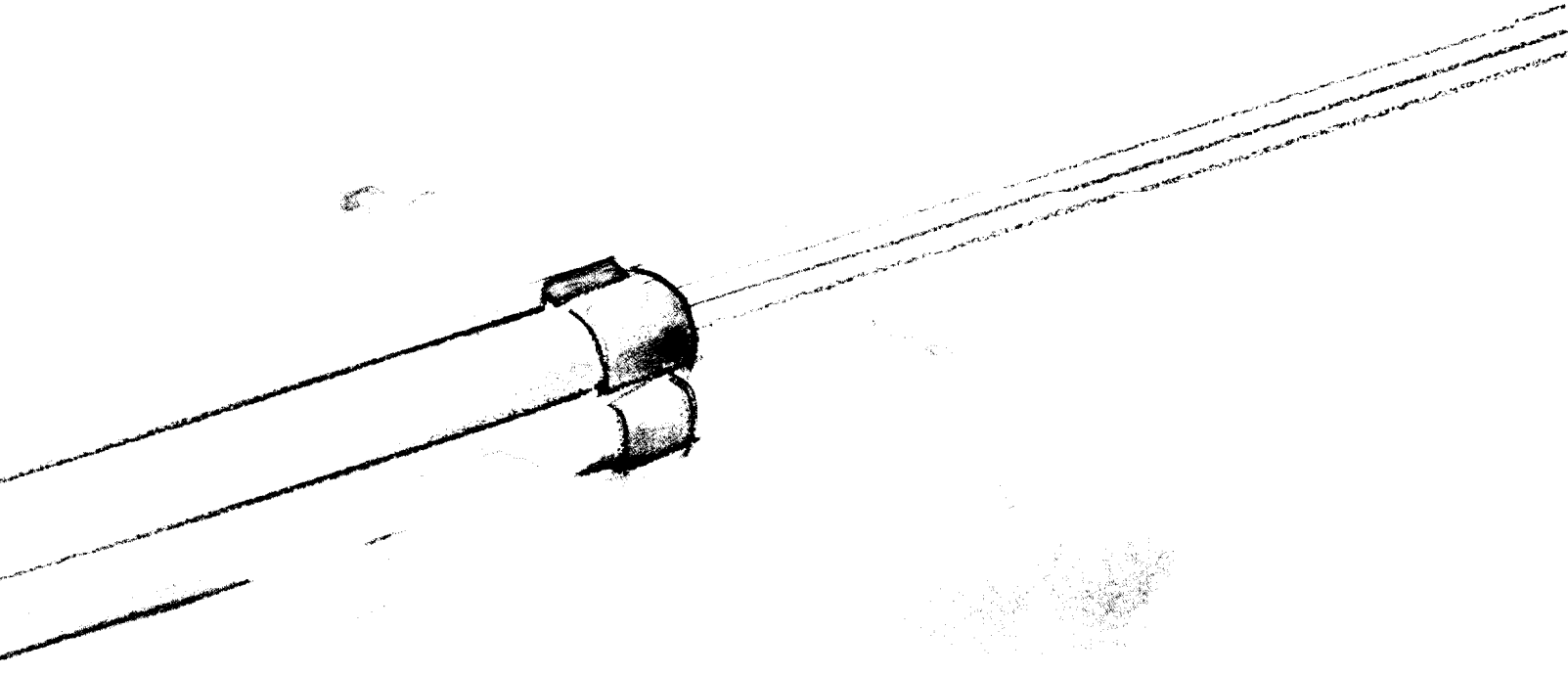

Opening figure (previous page): Looking between the dark pressure boundaries of a calculated supersonic jet, we see a radio-brightness map for a long extragalactic jet extending south some quarter of a million light-years from radio galaxy 3C200 and terminating in a radio lobe. In this map, which was taken at the Very Large Array (VLA) near Socorro, New Mexico, by Jack O. Burns, regions of high emission are depicted in red, intermediate emission in yellow, and low emission in blue. The jet powering the radio lobe north of the radio galaxy is for some mysterious reason not seen. *(Collage by Jim Cruz.)*

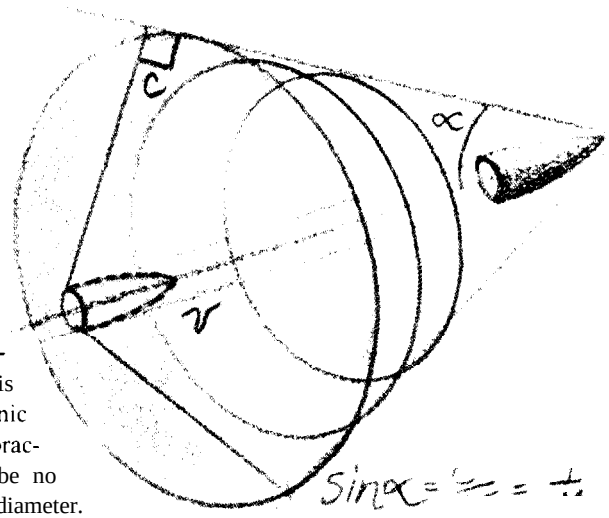

that so intrigued Ernst Mach that he set about to confirm it experimentally. Melsens conjectured that a high-speed projectile pushes ahead of itself a considerable mass of compressed air, which may cause explosion-like effects on the body it strikes. In other words, Melsens was proposing the existence of the bow shock that precedes a supersonic projectile, and, of course, Mach showed that Melsens was right.

In 1886 Mach and his experimental colleague Peter Salcher were the first to obtain schlieren photographs of a bow shock. These and other gas shocks are easy to record photographically because the abrupt change in density across a shock causes refraction anomalies in light transmitted through the shock. Mach correctly interpreted the bow shock as the envelope of sonic disturbances originating at the projectile. (The formation of shocks through convergence of sonic disturbances is discussed in Sidebar 2, "Shocks, Rarefactions, and Contact Discontinuities, ") He derived the famous equation sin a = c/v relating the Mach angle a (the opening half angle of the bow shock) to the projectile speed *v* and the ambient sound speed c (see drawing on this page).

Such a bow shock explains the first phenomenon. the double report: the first bang is produced by the powder gases escaping from the muzzle of the gun, and the second bang is the sonic boom associated with the bow shock of the supersonic projectile.

Ernst Mach is, of course, also remembered. for his principle of relativity (Mach's principle), which states that physical forces exist only because of the motion of matter relative to the rest of the matter in the universe. Mach's belief in the relative nature of physical laws must have played a role in the design of a novel setup for his ballistics experiments: he held the projectile fixed in the laboratory and fired air past *it* supersonically.

The supersonic air stream was produced by allowing highly compressed air to escape from a reservoir through a collimating de Laval nozzle. (Essentially the same apparatus is used today to produce supersonic gas jets in the laboratory.) For practical reasons the nozzle could be no more than a few centimeters in diameter. Mach quickly discovered that a projectile immersed in this modestly sized supersonic air stream created a network of standing shock waves far more complex than the single bow shock he expected (see Fig. A in Sidebar 3, "Steady-State Jets"). To quote the 1889 discovery paper of Mach and Salcher, "The stream exhibited a customary appearance so remarkable, that a detailed study of the jet itself seemed worthwhile." Such was the serendipitous discovery of the complex structure of supersonic gas jets and the beginning of a systematic research program carried out by Ernst Mach's son Ludwig to determine the properties of the jets. Further research was also carried out by Emden and Prandtl around the turn of the century.

Steady-State Supersonic Jets in the Modern Era

Interest in supersonic jets essentially vanished for two generations until World War II, when military considerations again made them the topic of research—this time at the Aberdeen Proving Grounds by a group of Americans who were investigating the phenomenon known as gun flash.

When an artillery piece fires, gas from the burnt powder exits from the cannon muzzle at supersonic speeds (the cause of the first bang) and produces for a brief instant the network of oblique crisscrossed shocks that Mach had discovered. These standing shock waves are set up by nonlinear radial oscillations of the gas jet caused by a pressure imbalance at the nozzle orifice (in this case the end of the muzzle). Of particular concern to the Aberdeen researchers was the occurrence in the jet of a type of shock known as a Mach disk. Mach disks, which are perpendicular to the jet flow and much stronger than the oblique shocks, produce "gun flash" by reheating the powder gas.

Since these flashes could reveal the position of a gun to the enemy, Ladenburg, Van Voorhis, and Winckler were interested in designing a muzzle to eliminate them. They discovered that the crucial parameter is the pressure ratio at the nozzle, that is, the ratio of the pressure of the gas in the jet to the pressure of the ambient, or atmospheric, gas. As shown in Sidebar 3, pressure ratios far from unity produce Mach disks, and pressure ratios near unity produce X-shaped "regular" shock reflections. To eliminate Mach disks, one need only flare the muzzle wall outward so that the emerging gas expands and repressurizes before reaching the atmosphere.

continued on page 45

Shock Waves versus Sound Waves

SIDEBAR 1

Explosions, projectiles whizzing by at supersonic speeds, high-speed collisions of solids—what do these phenomena have in common?

They all create very large changes in local pressure over very short times, and these violent pressure changes self-steepen into shock fronts, or shock waves. Unlike a sound wave, which is a small-amplitude compression wave that propagates at the local sound speed and leaves the state of the medium unchanged, a shock front is a nonlinear wave that abruptly changes the state of the supersonically approaching gas. The gas is generally at a higher temperature and pressure after it has passed through the shock (or. equivalently, after the shock has passed through the gas). Moreover, the shock-heated gas moves subsonically with respect to the shock. As we describe below, the narrow region defined as the shock front is a region where thermodynamic processes arc irreversible.

The cartoon from Courant and Friedrichs' classic book on supersonic flow illustrates the formation of a steep front in a discontinuous medium, namely, a train of skiers. The skiers, barreling single file down the narrow run. pile up in a heap as first one skier gets wrapped around a tree, and then, before he can warn the skier behind him to slow down, the next skier crashes into him, and so on. The pileup of human wreckage creates a steep front moving up the slope away from the tree analogous to a receding shock front. As in a continuous medium. formation of the front depends critically on the fact that the flow of skiers is "supersonic" in the sense that it is faster than the speed with which the medium, in this case the skiers, can respond to new boundary conditions. The high "pressure" of the skiers behind this front is analogous to the change of state experienced by shock-processed media.

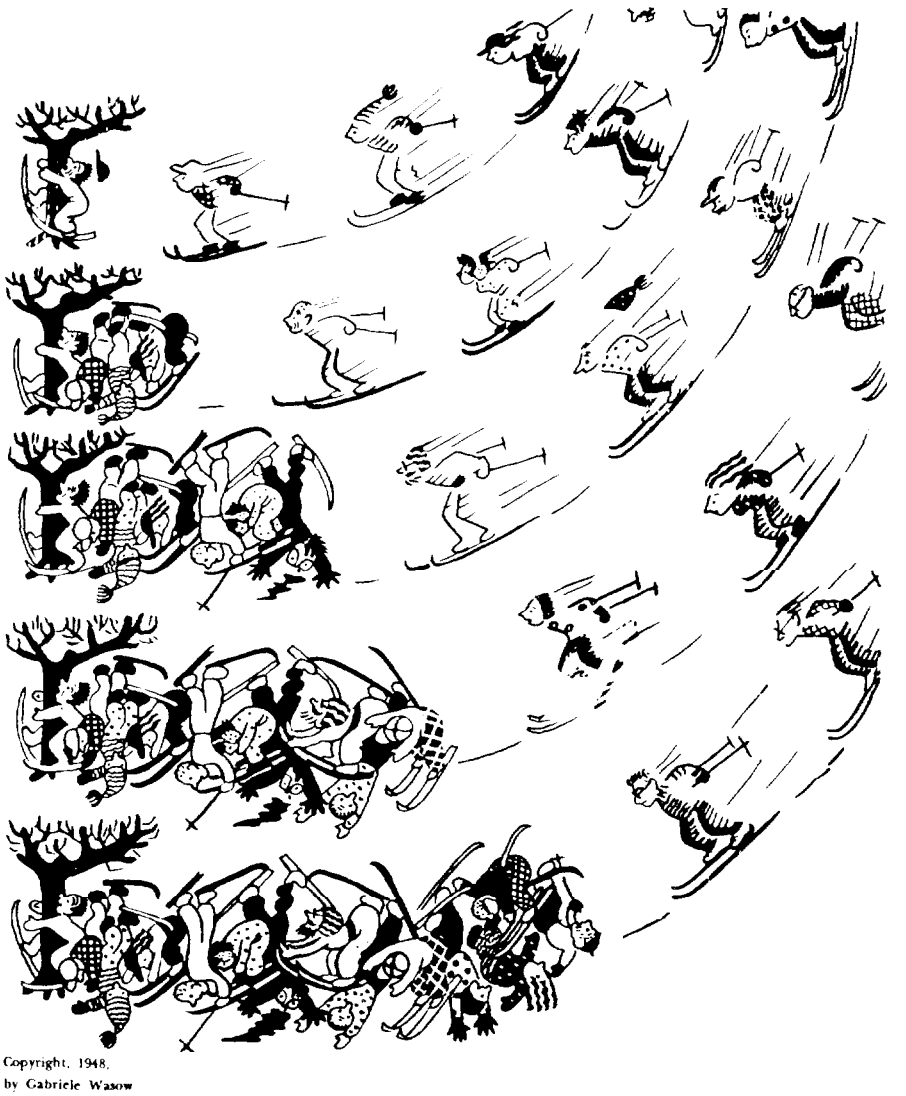

An example of a receding shock wave. From* Supersonic Flow and Shock Waves *by R. Courant and K. O. Friedrichs (New York:Interscience Publishers, Inc., 1948),

About a hundred years ago Stokes, Earnshaw, Riemann, Rankine, Hugoniot, and Lord Rayleigh deduced the conditions that prevail at shock fronts in gases. The framework they used to analyze this compressible flow are the equations of ideal gas dynamics. These nonlinear equations describe conservation of mass, momentum, and energy in an ideal fluid, a fluid in which all changes in kinetic and internal energy are due to pressure forces. Heat conduction and viscous stress are ignored and entropy is constant, so all thermodynamic changes are adiabatic and reversible. It was known that, within this context, infinitesimal pressure changes generate linear compression waves, better known as sound waves, that travel with the local sound speed c ($c^2 = (\partial P/\partial \rho)_S$). But what happens when the amplitude of a compression wave is finite?

Figure A illustrates what happens. At time t_i we have a finite-amplitude sound wave

such that the pressure variation δP is of order P. Variations in pressure imply variations in sound speed, since for an ideal gas $P \propto c^2$. Thus each point on the waveform propagates with its local sound speed, which is greater at the peaks than in the troughs. With time the waveform steepens (as shown at t_2) and eventually breaks (as shown at t_3) to produce multiple values for the state variables of the gas, P, p, and T. Of course this prediction is wrong. Instead nature inserts a shock front (dashed line) just before the wave breaks, and the flow variables remain single-valued.

How does this happen? On a microscopic level large gradients in temperature and velocity at the front of the steepening wave cause the irreversible processes of heat conduction and viscous stress to dominate in a region with a width equal to a few collision mean free paths and to counteract the self-steepening process so that a single-valued shock front forms. The net effect on a macroscopic level is that mass, momentum, and energy are conserved across the shock front, but entropy is not; it increases as relative kinetic energy is dissipated into heat through atomic or molecular collisions.

In 1864 Riemann was the first to analyze wave-steepening within the context of ideal gas dynamics. He mistakenly assumed that entropy was conserved (in other words, that all processes were adiabatic) across shock fronts as it is for finite-amplitude sound waves. Later, Rankine, Rayleigh, and Hugoniot showed that an adiabatic shock front would violate conservation of energy, and therefore shock fronts must be non-adiabatic and irreversible. Figure B shows the irreversible changes caused by the passage of a shock front in contrast to the reversible changes produced by a sound wave. To model these irreversible effects, the form of the Euler equations of gas dynamics we have adopted must be modified as described in Fig. 2 of the main text.

The dissipative nature of a shock front implies that it can maintain itself only in the presence of a driving force. A simple example of a driven shock front is given in Sidebar 2. ■

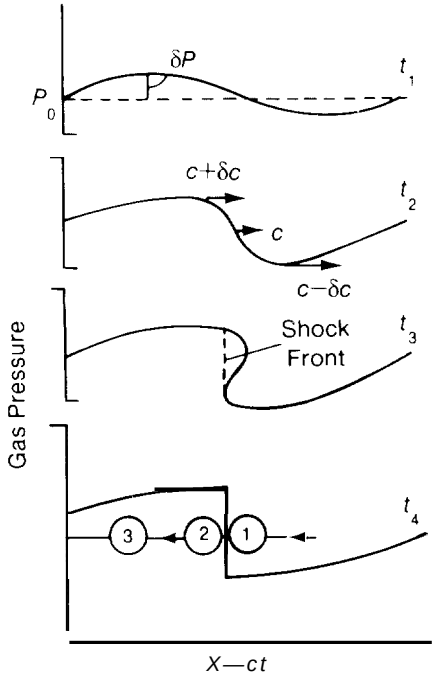

Fig. A. Self-steepening of a finite-amplitude sound wave. In the region where the state variables of the wave (here, pressure) would become multi-valued, irreversible processes dominate to create a steep, single-valued shock front (vertical dashed line).

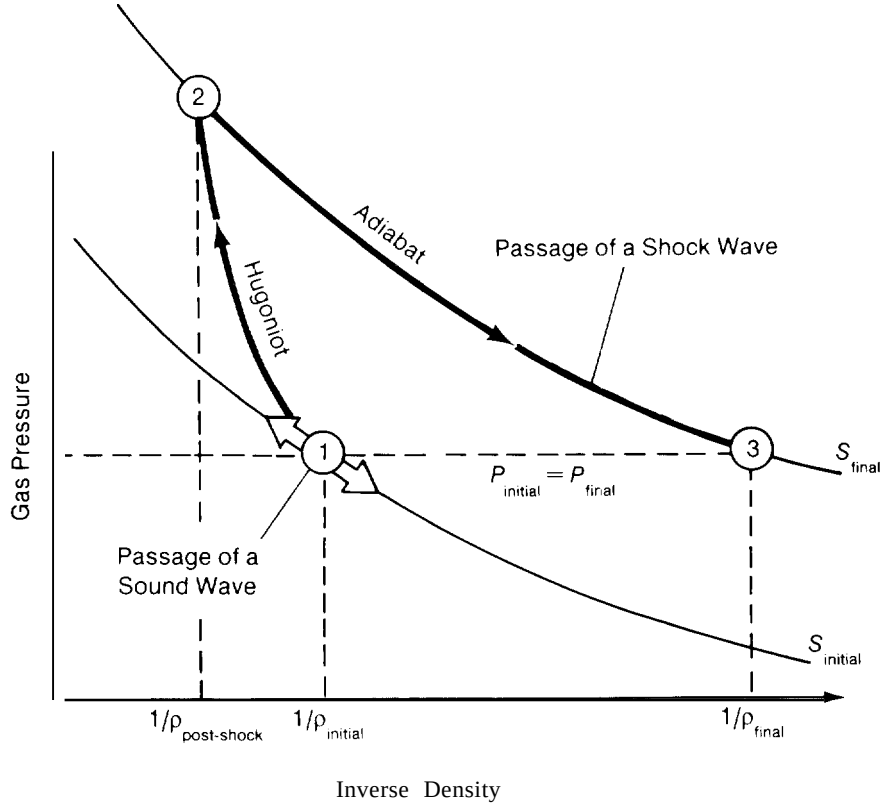

Fig. B, Effects of the passage of a sound wave and of a shock wave. As a sound wave passes through a gas, the pressure and density of the gas oscillates back and forth along an adiabat (a line of constant entropy], which is a reversible path. In contrast, the passage of a shock front causes the state of the gas to jump along an irreversible path from point 1 to point 2, that is, to a higher pressure, density,* and *entropy. The curve connecting these two points is called a Hugoniot, for it was Hugoniot (and simultaneously Rankine) who derived, from the conservation laws, the jump conditions for the state variables across a shock front, After passage of the shock, the gas relaxes back to point 3 along an adiabat, returning to its original pressure but to a higher temperature and entropy and a lower density. The shock has caused an irreversible change in the gas.

Shock Waves, Rarefactions, and Contact Discontinuities

SIDEBAR 2

The nonlinear equations of ideal gas dynamics support three types of nonlinear "waves": shock fronts. rarefactions, and contact discontinuities.

Contact discontinuities are surfaces that separate zones of different density and temperature. By definition such a surface is in pressure equilibrium, and no gas flows across it. When, as often happens, the tangential velocity of the gas on one side of the surface differs considerably from that of the gas on the other side, the surface is called a slip discontinuity. The boundary between a supersonic jet and the ambient gas is an example of a slip discontinuity.

The other two types of nonlinear waves arise from abrupt changes in pressure. Shock fronts accompany compression of the medium, and rarefactions accompany expansion of the medium. As a simple example of how these waves arise, consider the one-dimensional flow of gas in a small-diameter cylindrical tube, which is fitted with a piston atone end ($x = 0$) and closed at the other end. Figure A shows the time-dependent flow that results when the piston is suddenly pushed into the cylinder and how a shock front forms as sonic disturbances generated by the piston converge. These sound waves travel along trajectories called characteristic paths, or simply characteristics. In general, the characteristics of a set of hyperbolic partial differential equations are the paths along which certain variables are conserved and are thus the paths along which information travels. The characteristics for the equations of ideal gas dynamics are (1) the streamlines along which matter flows and entropy is conserved and (2) the PIUS and minus

Fig A. Compression in a Shock Tube

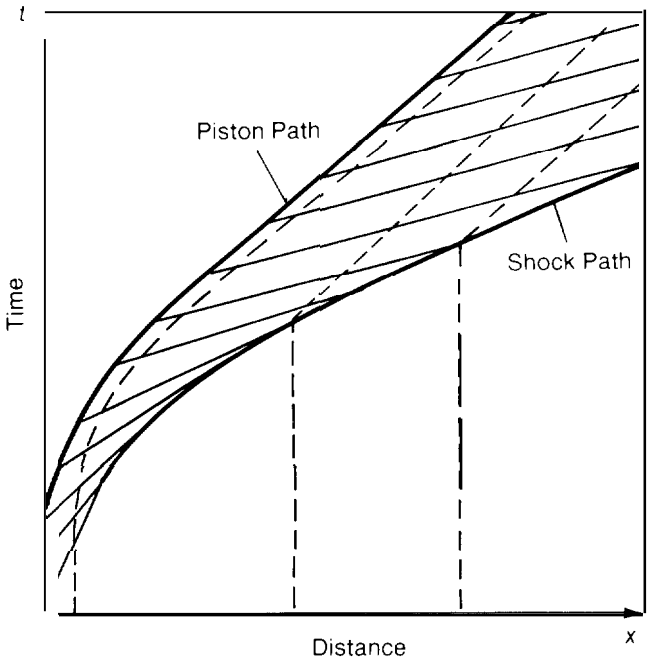

Fig B. Expansion in a Shock Tube

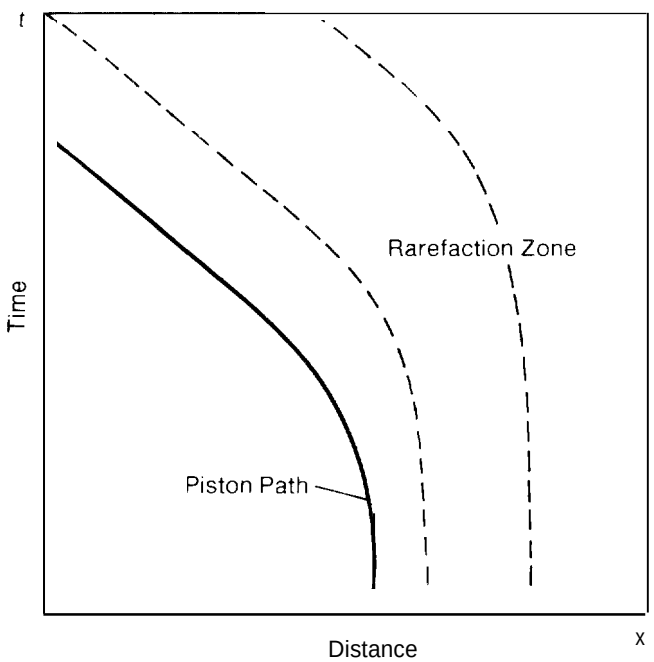

Characteristic Paths

Particle Paths

SIDEBAR 2

characteristics along which information travels from one point to another by sound waves, The so-called Riemann invariants, which are linear combinations of the fluid velocity and sound speed, are conserved along the plus and minus characteristics, In general, characteristics form a curvilinear coordinate system that reduces a complicated set of nonlinear partial differential equations to a coupled set of ordinary differential equations.

Since sonic disturbances travel in the gas at the local sound speed *c,* and since the gas immediately ahead of the piston is moving with the piston speed $v_{piston}(x)$, the sound waves emanating from each point along the piston path travel at a speed of $v_{piston}(x)$ + c. Hence at each point *x* the characteristic makes the same angle with the piston trajectory. As a result, the characteristics (red) emanating from the curved portion of the piston path (the acceleration phase) converge to form a shock front, (The bow shock of a supersonic projectile also forms where sonic disturbances generated along the trajectory converge, except that in this case the sonic disturbances move through a stationary rather than a moving medium and therefore all travel at speed c.) The shock front ahead of the piston travels along the tube at supersonic speeds. Gas particles farther away from the tube remain stationary until the shock front passes, and then they travel at a speed equal to the final constant speed of the piston. The closer spacing of the particle paths (dashed lines) gives graphic evidence of shock compression.

Figure B shows the time-dependent flow that results when the piston is suddenly withdrawn from some position within the cylinder. As in Fig. A, characteristics drawn at a constant angle to the piston path represent the path of sonic disturbances generated in the gas immediately adjacent to the piston. In this case the characteristics (blue) emanating from the curved portion of the piston path diverge to form a rarefaction zone (gray). The greater separation of the particle paths in the rarefaction zone indicates that the gas is expanding. ■

continued from page 41

Other data on supersonic flows arc available from studies of jet and rocket propulsion. Since these studies were aimed at designing more efficient, higher thrust engines, virtually all of them have focused on the steady-state, or time-averaged, properties of the jet flow, as has our discussion so far.

Time-Dependent Jets in Nature

The time-dependent evolution of-jets becomes important when we consider supersonic "jets" in nature. One example is the supersonic jet produced by the eruption of a gas-rich volcano, such as the eruptions of Krakatoa and Mount St. Helens. The blast wave that accompanies the formation of such a volcanic jet produces widespread devastation. Experiments have shown that these transient supersonic jets have structural properties resembling those of steady-state jets.

Other examples are the numerous jets emanating from astrophysical objects. In our galaxy protostars, old binary star systems associated with supernova remnants. and planetary nebulae produce jets of' ionized gases. A number of these stellar jets have knots of bright emission that remind one of the bright spots in the exhaust jet shown in Fig. 1, Spectral lines from highly excited atoms in the knots indicate that these bright spots are regions of high temperature, probably produced by shock heating. The Doppler shifts of the spectral lines demonstrate that these jets arc still evolving with time.

Our final example of time-dependent jets. and the ones that exhibit the most remarkable and mysterious stability, are the enormous jets emanating from quasars and other galaxies, These jets, known as radio jets because most of them can be observed only with radio telescopes, range from thousands to millions of light years in length, or about fifty to one hundred jet diameters. Many of them exhibit bright knots of radio emission in the beam. A radio jet typically ends in a "hot spot"-a small region of intense radio emission—embedded in a larger amorphous lobe of fainter emission (the opening illustration is an exception).

The emission spectra of radio jets, which are continuous and polarized, are produced by synchrotrons emission from a nonthermal population of relativistic electrons gyrating in a magnetic field. This nonthermal component probably coexists with a diffuse thermal plasma in some uncertain mixture to form the "stuff" of extragalactic radio sources. We know little else about the composition of the jets and the lobes and, in the absence of spectral lines, have no direct measure of jet speeds from Doppler shifts.

In a landmark paper, written in 1974 when only the radio lobes, and not the jets themselves, had been observed, Roger Blandford and Martin Rees interpreted the hot spots in the lobes as the point of impact of a supersonic gas jet impinging on the ambient medium as the jet advances. [n other words, the radio lobes are powered by fluid-like beams. or jets, originating at the centers of radio galaxies. They suggested that the main structural features of the jets could be explained by ideal gas dynamics, that is, by the nonlinear differential equations of compressible fluid flow. Magnetic fields and complex plasma dynamics that might affect local regions could be ignored when considering the overall structure of a jet,

The fluid-beam hypothesis of Blandford and Rees provides a simple physical explanation for radio observations and a framework for detailed model building, but within this framework the issue of stability becomes paramount. We know from laboratory experiments that Kelvin-Helmholtz shear instabilities grow rapidly on the boundary of supersonic gas jets and effectively decelerate and disrupt the flow. How do extragalactic jets propagate such great distances without suffering the same fate? Are they or are they not, governed primarily by the equations of gas dynamics'? If so, what are the critical parameters determining the stability and the observed morphology of the flow? We undertook to answer these questions by

continued on page 50

SIDEBAR 3

Steady-State Jets

Supersonic gas jets are created in the laboratory by allowing a highly compressed gas to escape through a nozzle into the atmosphere or some other ambient gas. In contrast to astrophysical jets, laboratory jets usually have high density ratios ($\eta \equiv \rho_{jet}/\rho_{ambient} > 1$), moderate Mach numbers ($M \equiv v_{jet}/c_{jet} \leq 3$), and large pressure mismatches at the source. Investigations of laboratory jets have, until recently, focused on their steady-state behavior rather than the initial time-dependent behavior of interest in astrophysical contexts. Nevertheless, our understanding of the steady-state structures observed in laboratory jets provides a point of departure for interpreting our numerical simulations of time-dependent jet flow.

An Idealized Supersonic Jet

Figure,4 shows the characteristic structure taken on by a slightly underexpanded supersonic jet, that is, one for which the pressure of the gas at the nozzle orifice. P.. is slightly greater than the ambient gas pressure, P_a. (A jet is referred to as underexpanded if $K \equiv P_n/P_a > 1$, overexpanded if $K < 1$, and pressure matched if $K = 1$.)

This complicated axisymmetric structure has several remarkable features. First, the jet boundary oscillates as the jet gas periodically overexpands and reconverges in its attempt to match the ambient pressure. The gas continually overshoots the equilibrium position because the effects of the boundary arc communicated to the interior of the jet by sound waves, which, by definition, travel more slowly than the bulk supersonic flow. The characteristic paths of the sound waves converge to form the second remarkable feature of the jet, the network of crisscrossed shock waves, or shock diamonds (red lines). These standing shocks alternate with rarefaction fans (blue lines). The gas in the jet interior expands and cools (shades of blue) as it flows through the rarefaction fans and is compressed and heats (shades of red) as it passes through the shock diamonds. The figure clearly illustrates that the jet interior is always out of step with the jet boundary. For example, the positions of greatest gas compression (dark red) do not coincide with the

SIDEBAR 3

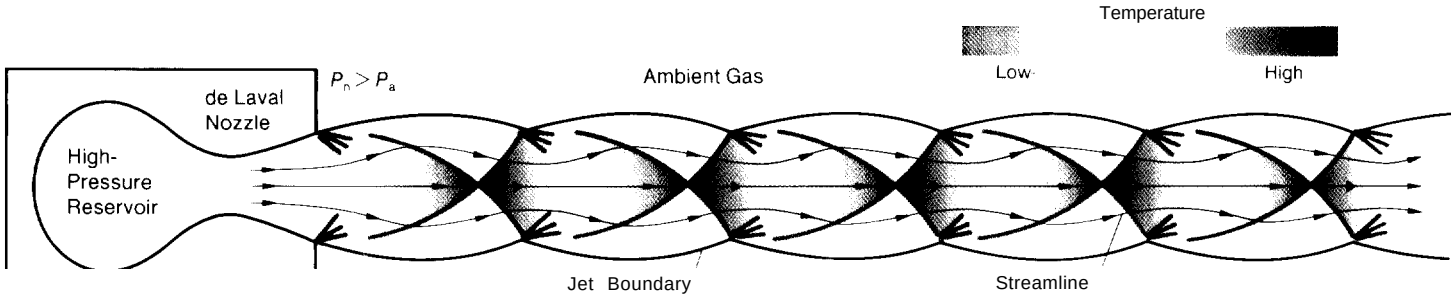

Fig. A. Idealized steady-state structure of a slightly underexpanded (P_n slightly greater than P_a) supersonic jet. The red lines represent incident and reflected shocks (see Fig. B), and the blue lines indicate the beginnings of rarefaction fans. The gas temperature varies according to the key. Black streamlines follow the oscillating flow path of the jet gas.

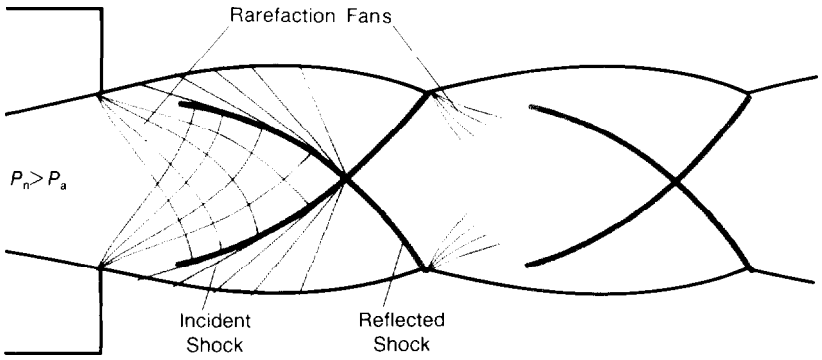

Fig. B. Regular reflection in a slightly underexpanded jet. The pattern of crisscrossed shocks in Fig. A can be understood in terms of characteristics. Diverging characteristics (blue) form rarefaction zones. Converging characteristics (red) from the boundary form the incident cortical shocks, which reflect off the jet axis to form the reflected shocks.

positions of minimum jet diameter. The black streamlines in the figure indicate the flow paths of the gas. The gas bends out toward the boundary as it passes through rare faction fans and bends back toward the axis as it passes through shock fronts.

Regular Reflections

Figure B shows how the shock structure in Fig. A can be understood in terms of characteristics. As the gas leaves the nozzle, it expands and a rarefaction fan (diverging blue characteristics) emanates from the nozzle orifice. The gas overexpands, and the pressure of the ambient gas at the boundary, acting like the piston in Sidebar 1, pushes the jet gas back toward the axis, creating the red characteristics. These characteristics form a converging conical shock. When this so-called incident shock reaches the jet axis it undergoes a regular reflection; that is, it forms a diverging shock. At the point where this reflected shock reaches the jet boundary, it knocks the boundary outward, creating a new rarefaction fan, and the process begins all over again. The geometric pattern of the *(x, y)* characteristics that form the shocks and rarefaction fans in this steady-state two. dimensional flow is similar to that of the

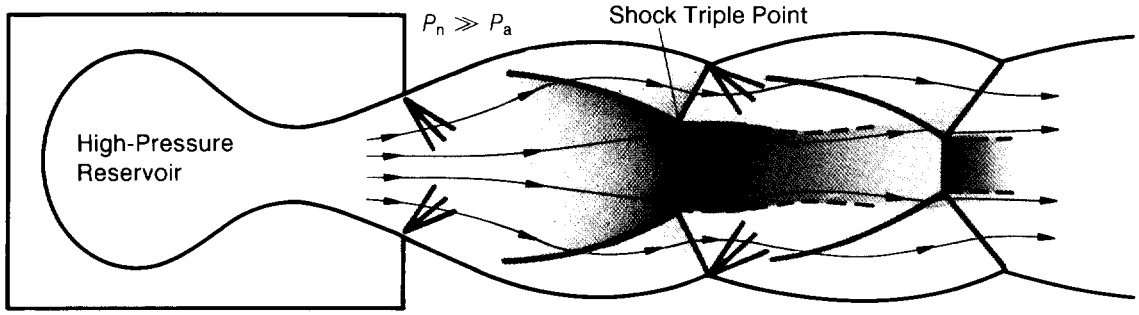

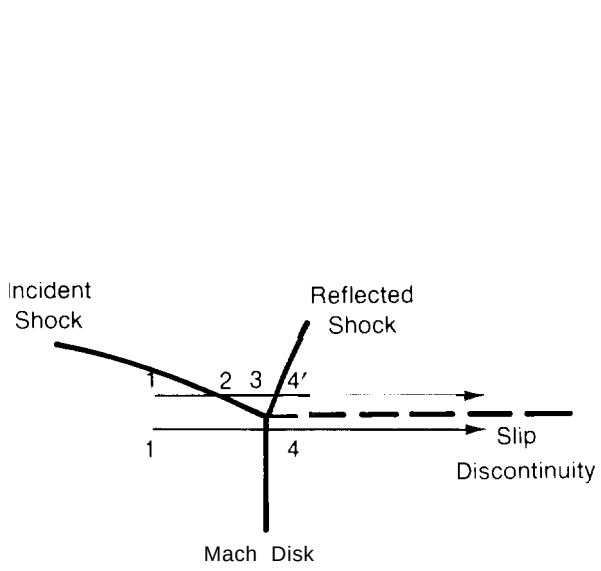

(1) Shock Triple Point

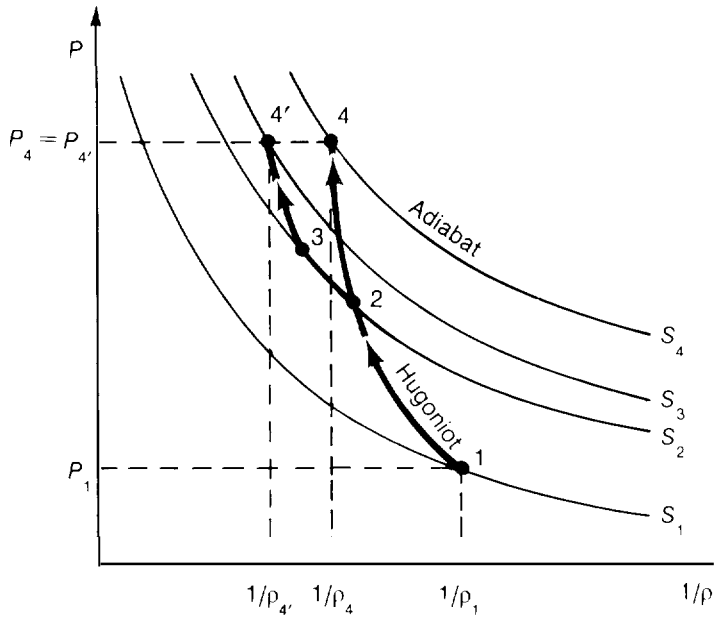

(2) Thermodynamic History

Fig. C. Mach reflection in an underexpanded ($P_n \gg P_a$) supersonic jet. A Mach reflection creates a shock triple point where three shocks meet. Figures C1 and C2 show how passage through the Mach disk {from point 1 to point 4) slows down the beam much more than passage through the incident and reflected shocks (from point 1 through points 2 and 3 to point 4'. As a result, a slip discontinuity is formed {dashed line).

(x, t) characteristics for one-dimensional time-dependent flow described in Sidebar 2.

Mach Reflections

A striking change in flow structure occurs when the pressure mismatch at the orifice is large ($K \gg 1$ or $K \ll 1$). As shown in Fig. C for an underexpanded jet, the incident shock, rather than converging to a point on the axis, reflects at the perimeter of a Mach disk—a strong shock normal to the flow direction (so named because Ernst Mach was the first to record its existence). The angle between the incident shock and the jet axis determines the type of reflection: small angles of incidence yield the regular reflections shown in Figs. A and B, and large angles of incidence yield Mach reflections. When gas passes through a shock, its velocity component normal to the shock is greatly reduced but its parallel component remains unchanged. Thus shocks with large angles of incidence relative to the flow axis are much more effective at slowing down the flow than shocks with small angles of incidence. The critical angle for transition from regular reflections to Mach reflections is approximately the angle that yields a sonic relative velocity for the gas downstream of the shock.

SIDE BAR 3

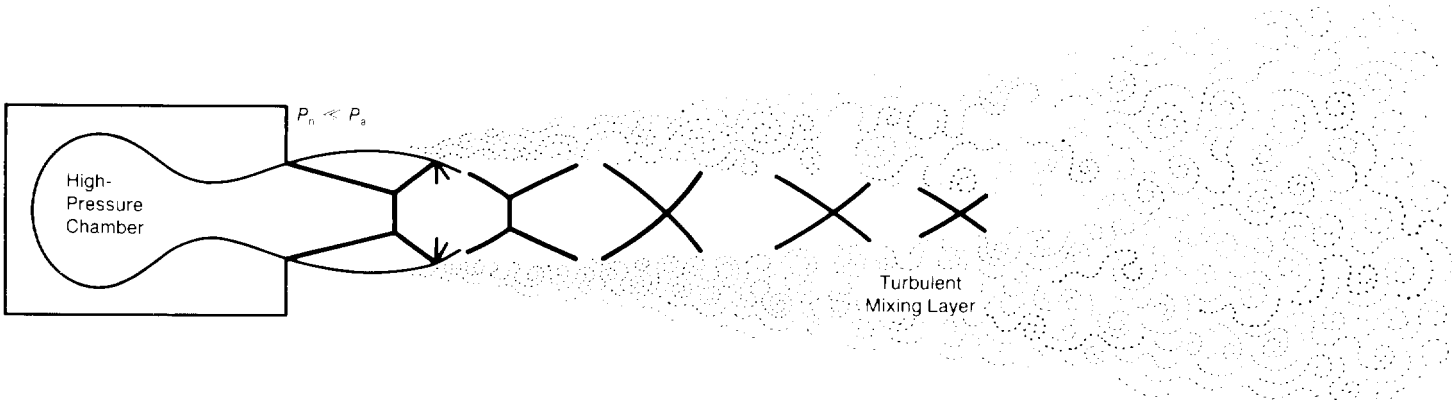

Fig. D, Realistic steady-state structure of an overexpanded ($P_n \ll P_a$) supersonic jet, showing the presence of both Mach reflections and regular reflections. Since this is an overexpanded jet, shocks rather than rarefactions emanate from the nozzle orifice. Shear instabilities create a mixing layer that grows until it reaches the beam axis.

A prominent feature of Mach reflections is the emergence of a slip discontinuity (dashed line) from the shock triple point where the incident shock, reflected shock, and Mach disk meet, The flow velocity, density, and temperature are discontinuous across this contact surface. This slip discontinuity arises because. the thermodynamic pathway through the incident and reflected shocks *does not equal* the pathway through the Mach disk.

In Fig. Cl we display two adjacent streamlines, one on each side of the shock triple point, and in Fig. C2 we display the corresponding thermodynamic pathways.

Adjacent fluid elements at some initial point on either streamline have the same state variables and the same total (kinetic plus internal) specific energy, that is, energy per unit mass. This quantity is given by

$$\frac{1}{2}v^2 + \frac{\gamma}{\gamma - 1}\frac{P}{\rho},$$

where y is the ratio of the specific heat of the fluid at constant pressure to the specific heat at constant volume.

By Bernoulli's principle the total specific energy remains constant along a streamline, Therefore, when the two adjacent fluid elements arrive at points 4 and 4' in Fig. Cl they must still have the same total specific energy. They must also have the same pressure because they are still adjacent. However, we see from Fig. C2 that their densities and entropies are different. The element at point 4 has been shock-heated along a Hugoniot to a higher entropy and lower density than the element that passed through the incident and reflected shocks along points 2 and 3 to point 4'. The lower density of the fluid element at point 4 implies that its internal energy (which is proportional to P/ρ) is greater than that of the fluid element at point 4'. Bernoulli's principle then implies that the fluid element at point 4 must have a correspondingly lower kinetic energy, and hence flow velocity, than the adjacent element at point 4'. A slip discontinuity results from this difference in flow velocities,

Laboratory Supersonic Jets

The jet structures shown in Figs. A, B, and Care idealizations in that real supersonic jets do not have sharp, stable boundaries but turbulent boundaries where jet and ambient gases mix. Figure D shows a more realistic steady-state structure for an overexpanded laboratory jet. Near the orifice, where the pressure mismatch is large, Mach reflections occur, but farther downstream the reflections are regular. The mixing layer, which grows as a result of Kelvin-Helmholtz (shear) instabilities, progressively eats its way into the supersonic core of the jet. When the mixing layer reaches the axis of the jet. the flow is subsonic and fully turbulent. It is then susceptible to twisting and bending motions, like a smokestack plume in a crosswind,

Strictly speaking the wave structures within the supersonic core are not steady since they are buffeted by the turbulent boundary layer. However, their average positions, those in Fig, D, are well defined. ■

continued, from page 45
solving the equations of gas dynamics through numerical simulation.

Numerical Jet Laboratory

The numerical problem we set ourselves is well defined. We start with the equations for compressible fluid flow displayed in Fig. 2a. assume that at $t = 0$ the jet gas starts to flow continuously through a narrow orifice into a region filled with quiescent gas as shown in Fig. 2b, and compute the time-dependent flow numerically with finite-difference techniques. We assume that the flow is axisymmetric and nonswirling (that is, the gas has zero angular momentum) and thus reduce a three-dimensional problem to two dimensions *(R* and *Z).* This reduction is necessary to achieve reliable numerical results with the computing power of a Cray-1. Moreover, since many extragalactic jets arc remarkably straight over most or all of their lengths, axisymmetry is a reasonable assumption. The importance of nonaxisymmetnc effects is discussed toward the end of this article.

The interesting thing about this problem is that it is scale-invariant, and therefore the results of the calculation can be scaled from laboratory to cosmic dimensions by varying the only dimension that appears in the problem, the jet diameter. Four scale-invariant (dimensionless) parameters determine the flow: η, *K, M,* and θ. The parameter η is the ratio of the beam, or jet, gas density ρ_b to the ambient gas density ρ_a,

$$\eta \equiv \rho_b / \rho_a ;$$

the parameter *K* is the ratio of the jet gas pressure P_b to the ambient gas pressure P_a,

$$K \equiv P_b / P_a ;$$

the parameter M, the Mach number. is the ratio of the jet speed v_b to the speed of sound in the jet gas c_b,

$$M \equiv v_b / c_b ;$$

(a) Euler Equations for Compressible Flow

Conservation of Mass
$$\frac{\partial \rho}{\partial t} + \nabla \cdot (\rho \mathbf{v}) = 0$$

Conservation of Momentum
$$\frac{\partial (\rho \mathbf{v})}{\partial t} + \nabla \cdot (\rho \mathbf{v} \cdot \mathbf{v}) + \nabla P = \vec{\mathcal{D}}$$

Internal Energy Equation
$$\frac{\partial (\rho e)}{\partial t} + \nabla \cdot (\rho e \mathbf{v}) + P(\nabla \cdot \mathbf{v}) = \mathcal{Q}$$

Equation of State for Ideal Gas
$$P = \rho c^2 / \gamma = (\gamma - 1)\, \rho e$$

ρ = density
v = velocity
P = pressure
e = internal specific energy
c = sound speed
γ = ratio of specific heats
$\vec{\mathcal{D}}$ = artificial viscous stress
$\mathcal{Q}$ = artificial viscous heating

(b) Computational Region

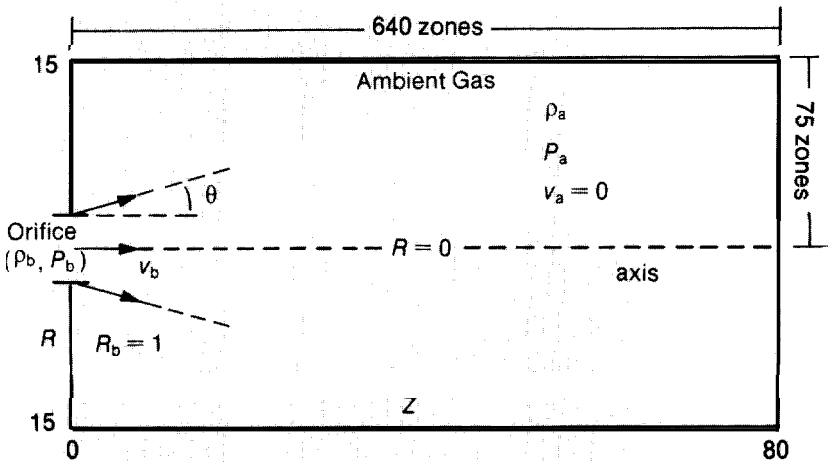

Inflow boundary conditions in terms of dimensionless parameters:
$\eta = \rho_b / \rho_a$, $M = v_b / c_a$, $K = P_b / P_a = 1$, $\theta = 0$.

Fig. 2. (a) The Euler equations of ideal compressible flow modified by source terms $\vec{\mathcal{D}}$ and $\mathcal{Q}$ to simulate viscous stress and heating in a narrow region behind the shock front. These terms have zero value elsewhere so that farther away from the shock front all processes are reversible and adiabatic, in agreement with experimental observations. (b) The computational grid and boundary conditions for numerical simulation of axisymmetric pressure-matched jets. Gas enters the computational region through a small orifice on the axis. Ambient gas is subsequently allowed to escape through the outer boundaries if required by advance of the jet.

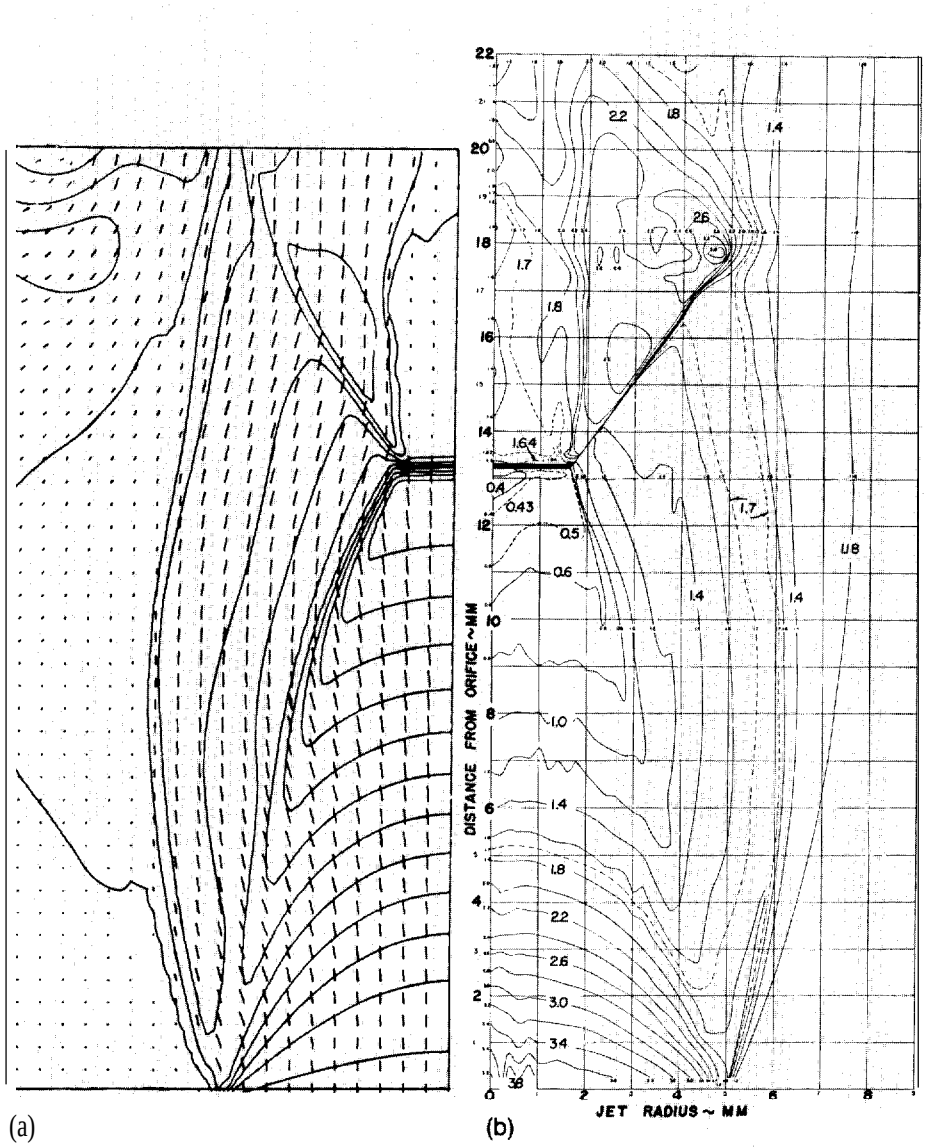

Fig. 3. A comparison of computed and measured steady-state flow fields in an underexpanded axisymmetric supersonic jet with parameters $\eta = 3.36$, $M = 1$, $K = 2.75$, and $\theta = 0$. The numerical solution given in (a) shows density contours and velocity vectors at every third grid point in a 60-by-180 calculation grid. The experimental results in (b), which* were *adapted from R. Ladenburg* et al., Physical Review *76(1949):662, show density contours and the triple-shock configuration. Note the good agreement between calculation and experiment on the position and geometry of the embedded shock waves.

and the parameter θ is the opening angle of the jet,

$$\vartheta \equiv \tan^{-1}(v_R / v_Z) ,$$

where v_R and v_z are the components of the beam velocity in the R and Z directions.

For extragalactic jets it is reasonable to reduce the number of parameters to two. To mimic the small observed opening angles of these jets. we start with a perfectly collimated beam at the source ($\theta = 0$). We also assume that the jet gas pressure equals the ambient gas pressure ($K = 1$) because x-ray data from satellites tell us that hot thermal gas pervades intergalactic space and is adequate in most cases to pressure-confine the jets. The remaining two-parameter set (M, η) defines a solution space that has scarcely been explored in the laboratory because of the difficulties of achieving very high Mach numbers ($M > 10$) and very low density ratios ($\eta \ll 1$). The ability to explore solutions corresponding to arbitrary values of these parameters is one of the great advantages of numerical simulation.

Solution of the two-fluid problem posed by jet flow depends critically on the motion of the interface separating the two fluids. Fluid interfaces are generally subject to Kelvin-Helmholtz instabilities, which are driven by shear motion parallel to the interface, and by Rayleigh-Taylor instabilities, which are driven by accelerations normal to the interface. Instabilities lead to mixing of the two fluids and can modify the jet flow significantly.

Techniques for tracking interfaces are a specialty at Los Alamos and Livermore. where complicated multi-fluid problems have been handled on large computers for three decades. Although multi-fluid problems are abundant in astrophysics as well, they have usually been approximated as one-fluid problems. Consequently, the use of interface-tracking techniques is somewhat of a novelty in numerical astrophysics, although in this application it is essential.

We adapted an interface-tracking technique developed by James M. LeBlanc and James R. Wilson at Livermore. This calculation is Eulerian; that is, the calculation grid is fixed. The interface between the two fluids is defined by those computational zones with fractional fluid volumes. The fractional volumes are carried along by the bulk flow, and their consequent redistribution on the grid is then used to construct an approximate geometry of the displaced fluid interface, Although an approximate treatment, the technique is robust and very effective at preventing an undesirable consequence of most Eulerian computations, the artificial "blending" of disparate materials at moving boundaries.

We tested the code through comparisons with experiment. Figure 3 shows one such comparison, in which we attempted to reproduce not only the general shape of the flow, but also the position and geometry of the embedded shock waves. The surprisingly good agreement gives us confidence that we can reproduce accurately the steady-flow structures measured in laboratory supersonic jet experiments and, with perhaps some luck, the transient jet structures as well.

A Supersonic Jet Up Close

Having described our numerical simulation apparatus, let us now use it to observe the establishment and propagation of a pressure-matched supersonic jet, that is, one for which $K = 1$.The following analysis relies heavily on computer graphics. Plots of several different flow variables will be required to get a complete picture of the flow and to dig out the essential physics.

Figure 4 shows four snapshots in the time evolution of a low-density jet with initial values of $(M,\eta) = (3,0.1)$. In these plots the color-coded density values show that the entire jet is substantially less dense than the ambient gas throughout its evolution. Pressure confinement is nevertheless maintained because the jet gas is correspondingly hotter than the ambient gas.

The penetration of hot, diffuse supersonic jets into cold, dense continuous media is just beginning to be investigated in the laboratory (Fig. 5), but this physical situation appears to be the relevant one for astrophysics. A novel aspect of such jets, already predicted by Blandford and Rees in 1974, is the establishment of a cocoon—a sheath of gas surrounding the central beam that "splashes back" from the head of the jet. The cocoon is visible in Fig. 4a as a blue layer above and below the green supersonic beam. The mechanics governing deflection of the beam gas into the cocoon at the so-called working surface is quite complicated and will be discussed below. Nevertheless, the existence of cocoons in low-density jets is easy to understand on simple physical grounds.

As shown in Fig. 6, the jet head advances at a speed determined by a balance of ram pressure (or, equivalently, momentum flux) along the beam axis in the rest frame of the working surface. If we let W be the speed of advance of the working surface, then ram-pressure balance is given by $\rho_b (v_b - W)^2 = \rho_a W^2$. Solving for W and using the definition $\eta \equiv \rho_b / \rho_a$, we find that

$$W = \frac{v_b \sqrt{\eta}}{1 + \sqrt{\eta}}. \qquad (1)$$

Equation 1 implies that the advance speed W

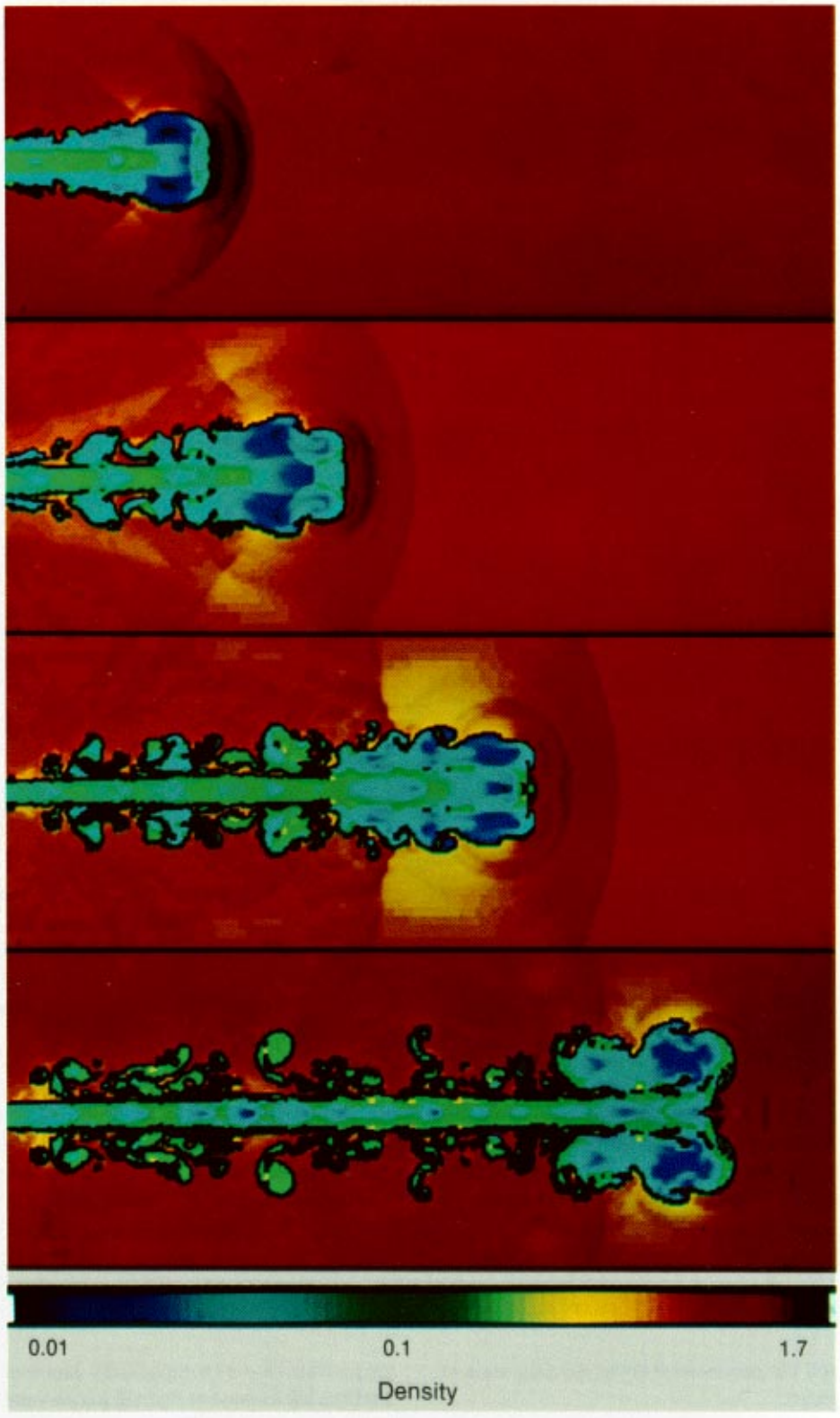

Fig. 4. Numerical simulation of the time evolution of a pressure-matched ($K = 1$) axisymmetric supersonic jet. The jet gas is admitted continuously from the left with an opening angle θ of zero. For this jet $M = 3$ and $\eta = 0.1$. The calculated gas density varies according to the color code. Frames (a) and (b) show the establishment and turnover of the jet cocoon, which is composed of gas that has passed through the terminus of the jet. Frames (c) and (d) show the subsequent mixing of cocoon and ambient gases, which leaves intact only a lobe of cocoon gas at the jet head. The bow shock driven by the supersonically advancing jet head is revealed by the jump in density it produces. The jet image has been reflected about the axis of symmetry for ease of visualization.

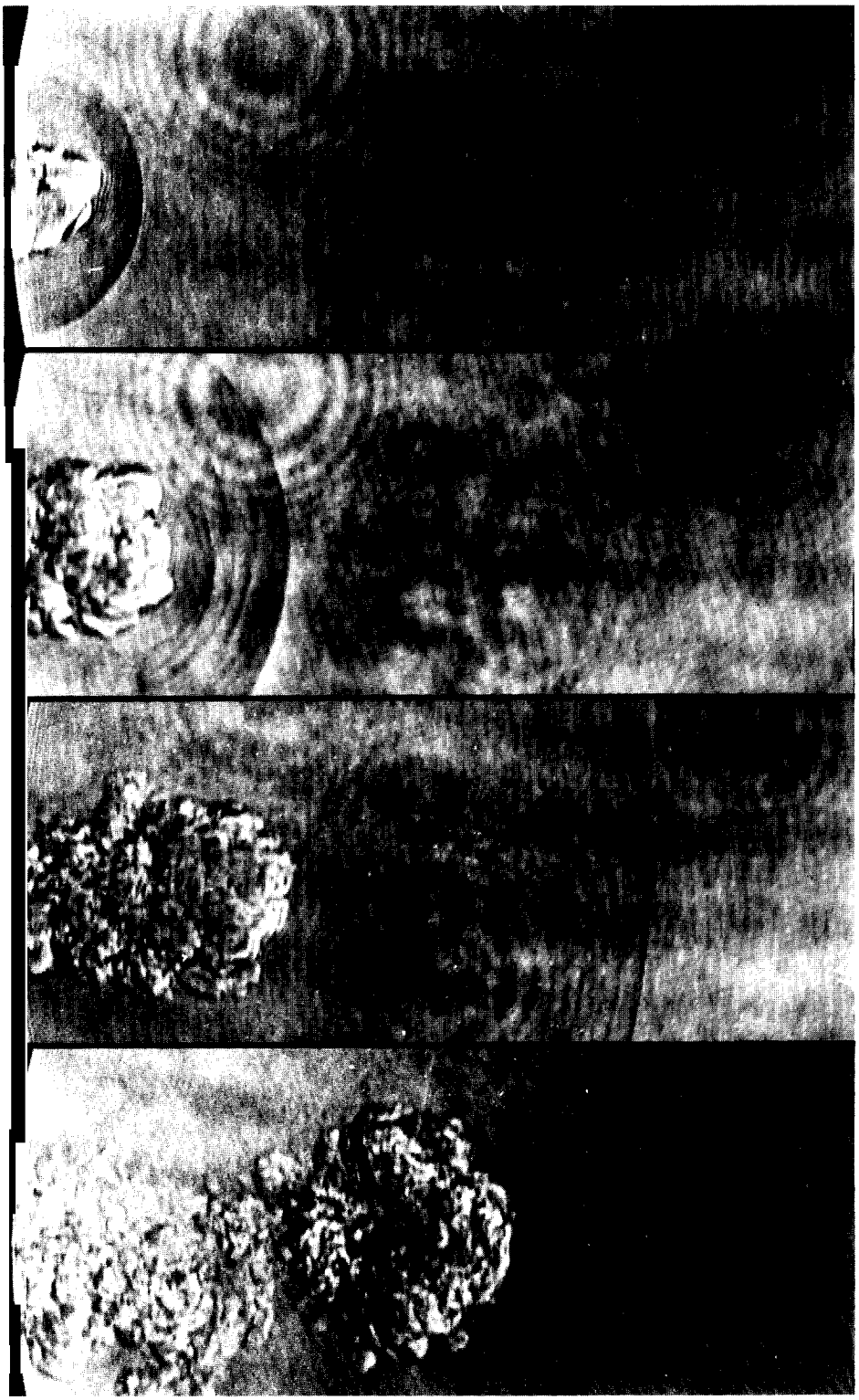

Fig. 5. Laser-schlieren photographs of the time evolution of a low-density supersonic jet. The jet was created by release of 3 joules of energy in a spark, which caused ejection of a plasma pulse into ambient air. Shown here, top to bottom, are short-exposure photographs taken 15, 35, and 80 microseconds after the pulse and at a very late stage in the evolution of the jet. The short exposure time reveals the transient behavior of the flow and emphasizes the turbulent structure of the jet cocoon. The bow shock preceding the jet can be seen as an expanding arc in the first three frames; it has moved out of view in the last frame. The length of the area viewed is 4.5 centimeters. (Reproduced with the permission of J. A. Cavolowsky and A. K. Oppenheim, Department of Mechanical Engineering, University of California, Berkeley.)

of the head of a diffuse jet ($\eta \ll 1$) is less than the beam speed v_b, which means that the beam gas constantly overtakes the jet head. Rather than accumulate there, the incoming beam gas continuously escapes into the cocoon after being shock-decelerated and deflected sideways at the working surface. Surprisingly, the cocoon gas actually flows backward toward the inlet. Backflow is a simple consequence of mass conservation and is encountered on earth when supersonic water jets are used to drill into rocks.

The relative velocity between the backward flowing cocoon gas and the ambient gas at the cocoon boundary is substantial. but it is subsonic for the jet shown in Fig. 4. Consequently, the cocoon boundary is subject to the Kelvin-Helmholtz shear instability. which overturns and mixes the cocoon and ambient gases, as can be seen in Figs. 4b and 4c. As a result of the instability, only a lobe of cocoon gas is left intact at the jet head in Fig. 4d. The central supersonic beam nevertheless appears to propagate without significant mixing at its boundary. We can verify that this is indeed the case with the aid of additional plots that elucidate the flow field in the jet (Fig. 7).

Details of the Flow Field

In Fig. 7a a novel mode of display reveals the large-scale structures of the flow field for he ($M = 3, \eta = 0.1$) jet of Fig. 4. Kinematically distinct parts of the flow inside and outside the jet are assigned different colors. Within the jet boundary (black) we can identify the central supersonic beam green), the backward flowing ($v_Z < 0$) cocoon gas (white), and the forward flowing ($v_z > 0$) cocoon gas (yellow). Outside the jet we can identify the undisturbed ambient gas (dark blue) and the bow shock (red). The beam consists by definition of those regions where the local kinetic energy flux ½ pv_z^3 is at least 5 percent of its maximum value. Aside from a few yellow patches within the beam, which wc shall comment on below, we can follow the supersonic channel uninterrupted to the very end of the jet.

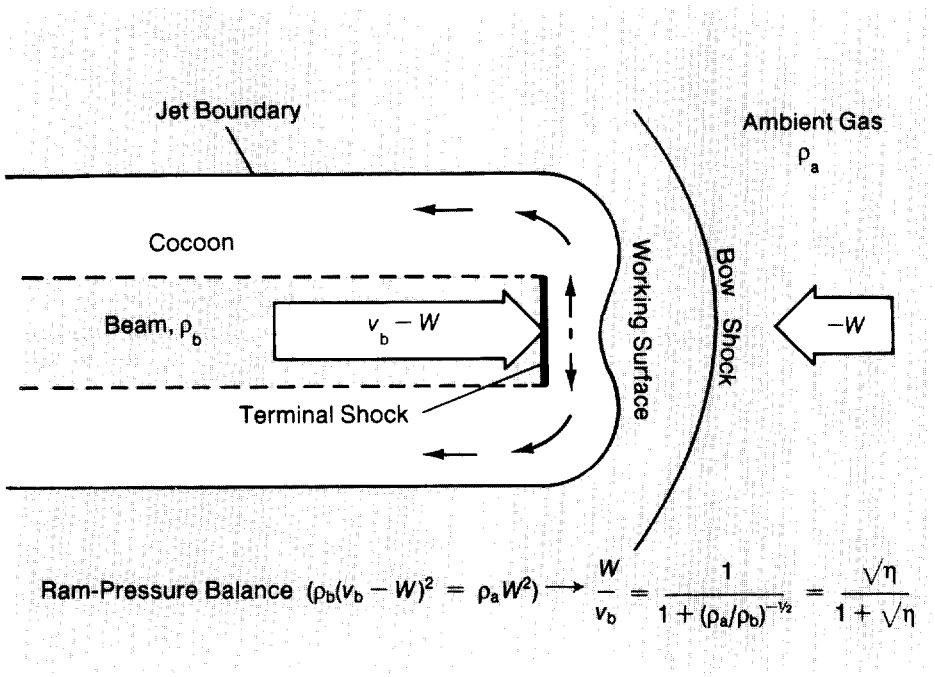

Fig. 6. Flow schematic of the jet head in the rest frame of the working surface. The speed of advance W of the working surface is determined by equating the ram pressure, or momentum flux, of the beam to the ram pressure of the ambient gas in a frame in which the working surface is stationary. In this frame the beam speed is v_b — W and the speed of the ambient gas is — W. The expression derived for W/v_b implies that, for jets with low density ratios ($\eta \ll 1$), the working surface advances much more slowly than the beam gas. However, the beam gas does not collect at the working surface but is shock decelerated and deflected sideways to form a low-density backward flowing cocoon around the forward moving beam.

Fig. 7. Computer-graphic diagnostics of the flow field at t = 60 for the (M= 3,n = 0.1) jet of Fig. 4. (a) The kinematic plot depicts cinematically distinct regions in different colors. *The beam boundary (black) encloses the beam (green), which by definition consists of those* regions *for which the kinetic energy flux* ½pv³ *exceeds 5 percent of the global maximum of that quantity. The backward flowing ($v_z <$ O) and forward flowing ($v_z >$ 0) cocoon regions are shown in white and yellow, respectively. The undisturbed ambient gas is dark blue, and the bow shock is red. (b) The vorticity plot depicts regions of large positive and negative azimuthal vorticity ($\nabla \times \mathbf{v})_\theta$ in green and yellow, respectively, and reveals the vortex sheet at the beam boundary (green) and the shear layer at the cocoon boundary (yellow). (c) The divergence plot depicts regions of large positive and negative divergence of the velocity ($\nabla \cdot \mathbf{v}$) in blue and red, respectively, and reveals a network of internal shock waves (red) and rarefaction zones (blue). (d) The temperature plot reveals the alternate heating and cooling of the gas by shock and rarefaction waves, respectively.*

The stability of the beam boundary is verified in Fig, 7b, where we plot the azimuthal vorticity $(\nabla \times \mathbf{v})_\theta$. Regions with a large positive vorticity are green, and regions with a large negative vorticity are yellow. The beam boundary, a region of high positive vorticity (shear). can be seen as a stable green layer, just inside the black jet boundary, that continues beneath the forward cocoon lobe up to the working surface. Note the coincidence of the beam boundary as defined by the two complementary techniques of Figs. 7a and 7b. At the end of the jet, the shear layer is carried into the cocoon, where it breaks up into isolated vortices. The existence of vortices in the cocoons of diffuse jets is one of our general findings and accounts for the forward flowing cocoon gas indicated in yellow in Fig. 7a.

In addition to positive vorticity, Fig. 7b reveals that a substantial amount of negative vorticity is being created within the beam. What is the mechanism responsible for this'? The answer is given in Fig. 7c, where regions of large positive flow divergence $\nabla \cdot \mathbf{v}$ are colored blue, and regions of large negative $\nabla \cdot \mathbf{v}$ are colored red. The blue regions are rarefaction zones, and the red regions encompass shock waves (see Sidebars 2 and 3). We see within the beam a well-developed network of crisscrossing shock waves separated by strong rarefaction zones. The negative vorticity is generated by the oblique shock waves. which are highly nonuniform in strength because of their cylindrical convergence toward the axis. The terminal shock at the working surface can also be seen in Fig. 7c just behind the leading contact surface. which is more or less normal to the incoming beam. This leading contact discontinuity separates the jet from the ambient gas. It propagates into the ambient gas, and no gas flows across it in either direction.

A color-coded temperature plot (Fig. 7d) clearly shows that the effect of the embedded shock waves is to compress and heat the beam gas. Knots of shock-heated gas can be seen downstream of each oblique shock intersection. Such knots frequently appear in supersonic rocket plumes as bright patches, which are due to enhanced thermal emission or to chemiluminescence.

Although the shock pattern in our simulation of a pressure-matched jet bears remarkable similarities to the shock waves characteristic of the overexpanded and underexpanded jets produced in the laboratory (see Sidebar 3), there is a vital difference. In the laboratory jets the shock pattern is stationary, whereas in the pressure-matched jet it moves downstream at a speed equal to a significant fraction of the beam speed. We shall return to this point later.

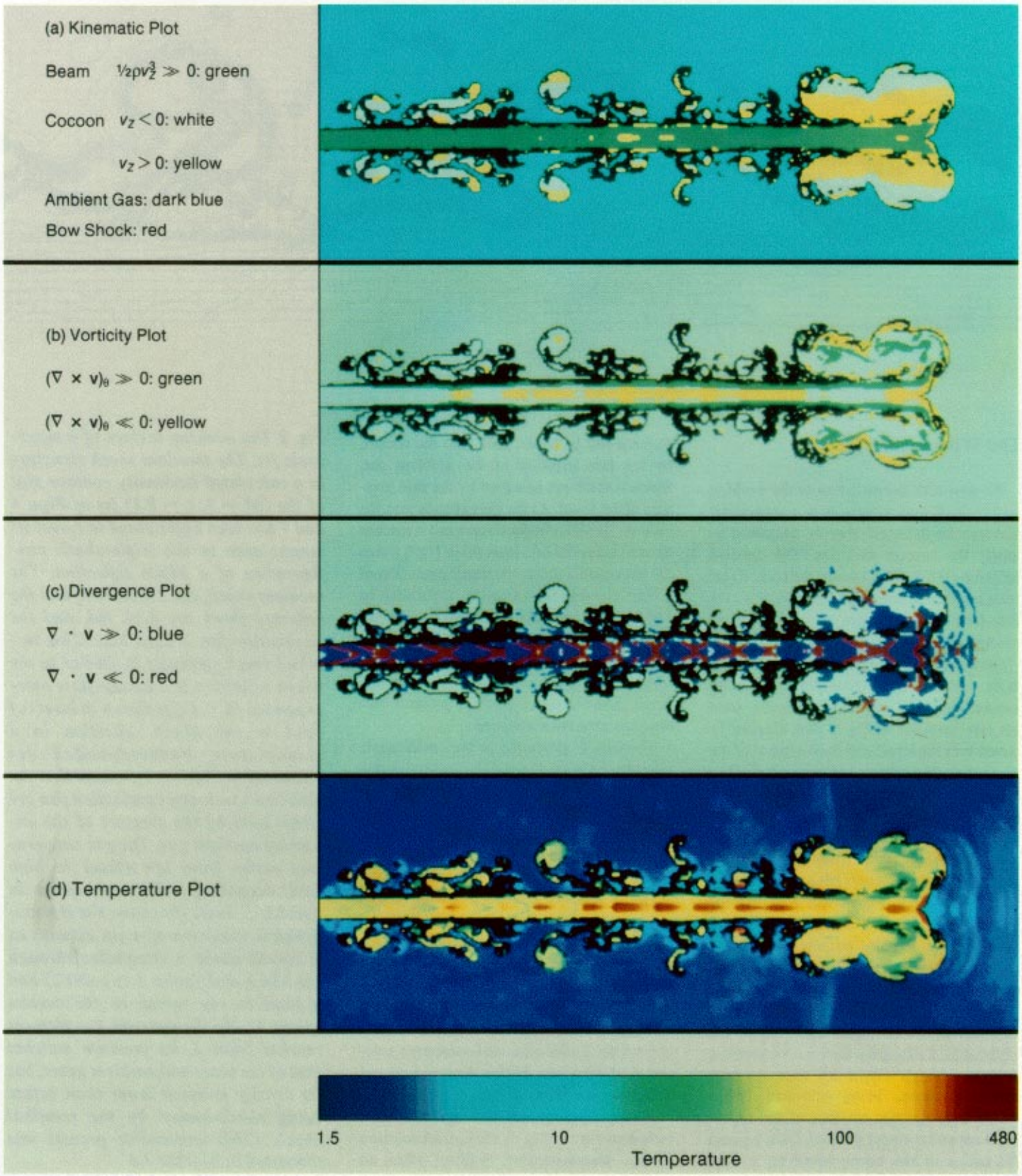
(a) Kinematic Plot
Beam $\frac{1}{2}\rho v_z^3 \gg 0$: green
Cocoon $v_z < 0$: white
$v_z > 0$: yellow
Ambient Gas: dark blue
Bow Shock: red
(b) Vorticity Plot
$(\nabla \times \mathbf{v})_\theta \gg 0$: green
$(\nabla \times \mathbf{v})_\theta \ll 0$: yellow
(c) Divergence Plot
$\nabla \cdot \mathbf{v} \gg 0$: blue
$\nabla \cdot \mathbf{v} \ll 0$: red
(d) Temperature Plot
1.5
10
100
480
Temperature

Airbrush illustrations in this article by Jim Cruz.

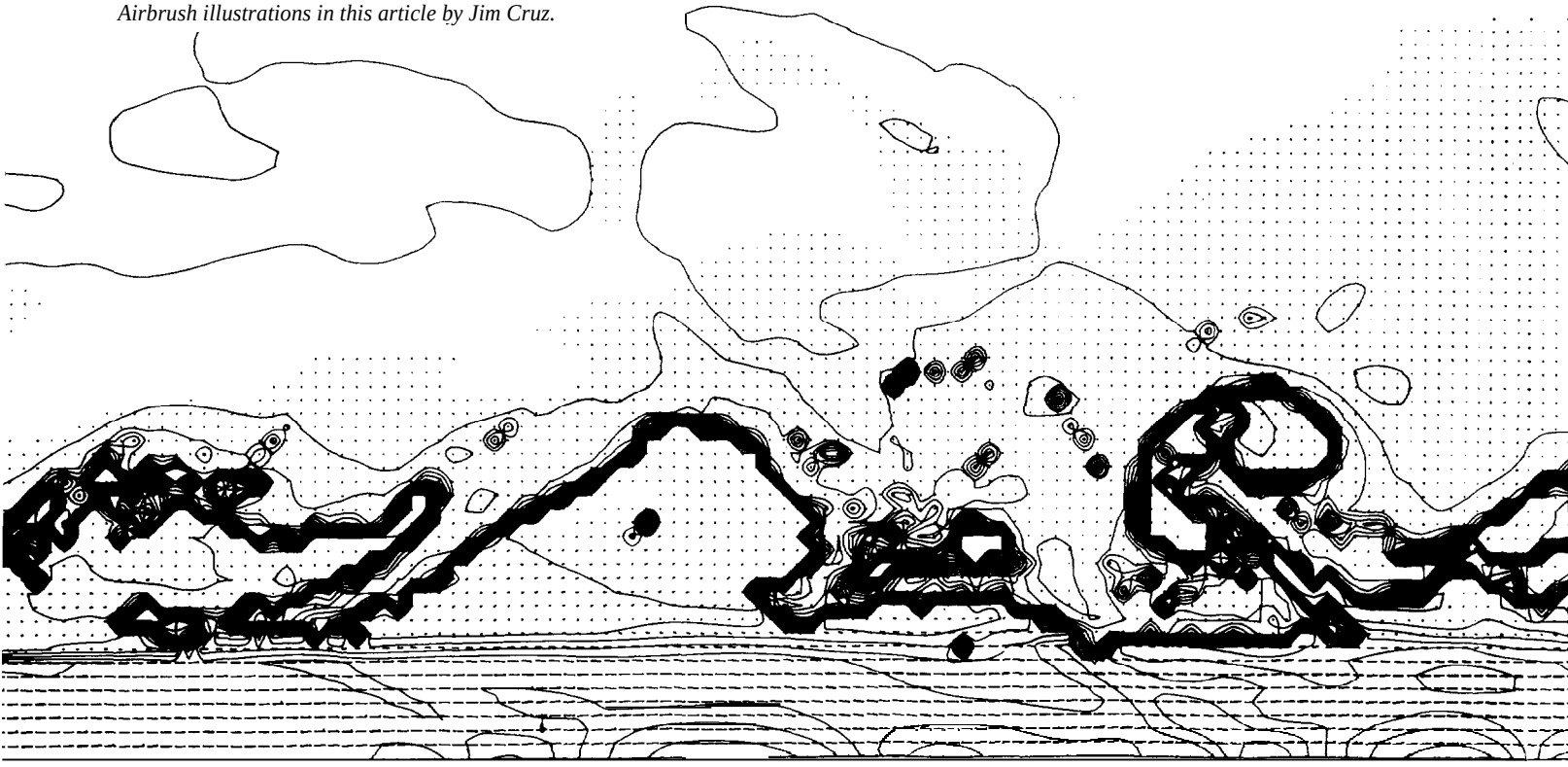

The Working Surface

We now turn our attention to the working surface itself and inquire how a supersonic flow can be deflected sharply backward to supply the cocoon with gas. The detailed structure of the working surface (Fig. 8) reveals a complex network of nonlinear waves and flow patterns that propagates as a coherent whole at the head of the jet.

Quite generally, the terminal shock system looks just like the triple-shock structure formed by Mach reflection in steady-state jets (see inset (a) in Fig. 8 and Sidebar 3), except that the structures downstream of the Mach disk (the reflected shock and rarefaction zones) are swept back by the oncoming ambient gas. Upon passing through the Mach disk, beam gas is virtually brought to rest with respect to the leading contact discontinuity, which is itself advancing into the ambient gas. The Mach disk converts the directed kinetic energy of the beam into internal energy, thereby creating a region of very high pressure and temperature between the Mach disk and the contact discontinuity. It is generally believed that this region corresponds to the hot spots observed in the radio lobes of extragalactic jets. The shocked high-pressure gas within this zone can only escape sideways, being confined longitudinally by the ram pressure of the opposing beam and ambient streams. Once beyond the radius of the beam, however, a fluid element will be blown back into the cocoon by the ram pressure of the ambient gas, which is there not balanced by the ram pressure of the beam. As the gas expands into the cocoon, its pressure decreases until it reaches the ambient pressure. Inset (b) in Fig. 8 traces the irreversible thermodynamic evolution of a fluid element following the streamline in Fig. 8 that passes through the Mach disk and into the cocoon. A key consequence of the irreversible nature of the terminal shock front is that the cocoon gas is generally less dense than the beam gas after pressure balance has been re-established.

Vorticity is generated at the shock triple point in the form of a slip discontinuity (the dashed line in Fig. 8), is carried into the cocoon, and contributes to the formation of a large-scale toroidal vortex surrounding the beam. The streamline in Fig. 8 that flows above the shock triple point circles the vortex to produce a forward flowing stream of high-pressure cocoon gas. This high-pressure environment in the cocoon drives the oblique incident-shock component of the beam's terminal triple shock. This intimate relation between the flow structures at the working surface and the adjacent cocoon constitutes a nonlinear self-consistent solution to the problem of flow deceleration and deflection in supersonic jets.

How can we be sure that our numerical techniques are giving us the correct solution to this time-dependent problem when no

***Fig. 8** The working surface of a supersonic jet. The terminal shock structure in a calculated isodensity contour plot of the (M = 3, n = 0.1) jet of Figs. 4 and 7 has been highlighted to reveal its resemblance to the triple-shock configuration of a Mach reflection. The incident shock, the Mach disk, and the reflected shock are dark red, and the rarefaction fan is dark blue. This terminal shock structure is similar to the Mach reflection in a steady-state overexpanded (K< 1) jet shown in inset (a) (and to the Mach reflection in a steady-state underexpanded jet presented in Sidebar 3), except that the reflected shock and rarefaction fan are swept back by the pressure of the oncoming ambient gas. The gas temperature varies from low (blue) to high (red) according to the scale shown in Sidebar 3. Inset (b) shows the thermodynamic evolution of a gas element as it travels along a streamline through the Mach disk (point 1 to point 2) and around to the vortex in the cocoon (point 3). By the time the gas element reaches point 3, its pressure matches that of the beam and ambient gases, but its density is much* **lower** *than before being shock-heated by the terminal shock. (This irreversible process was discussed in Sidebar 1.)*

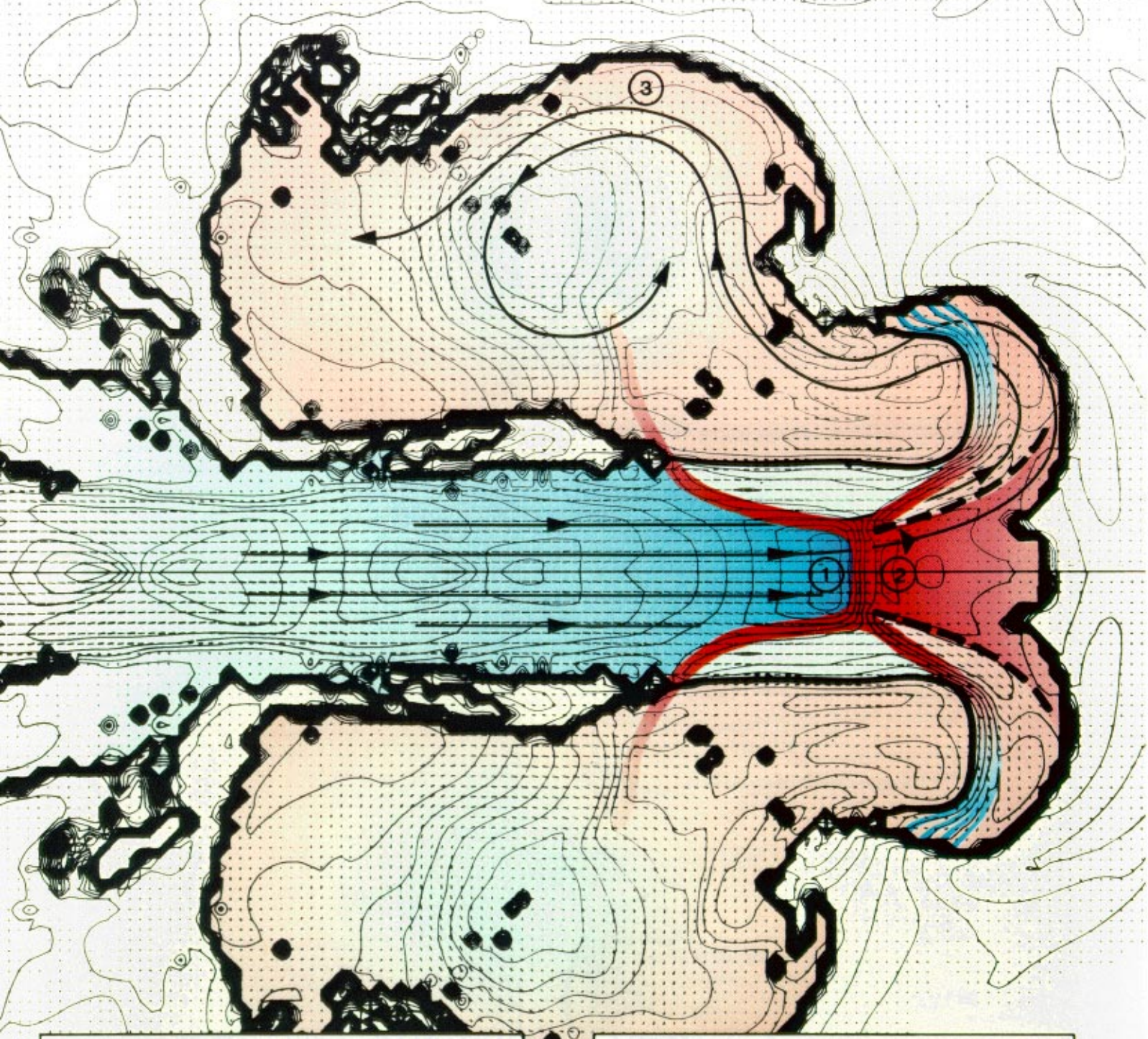

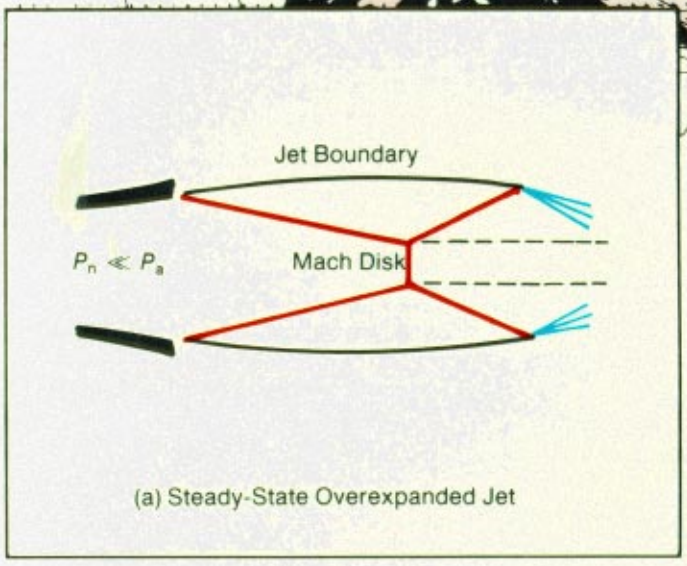

(a) Steady-State Overexpanded Jet

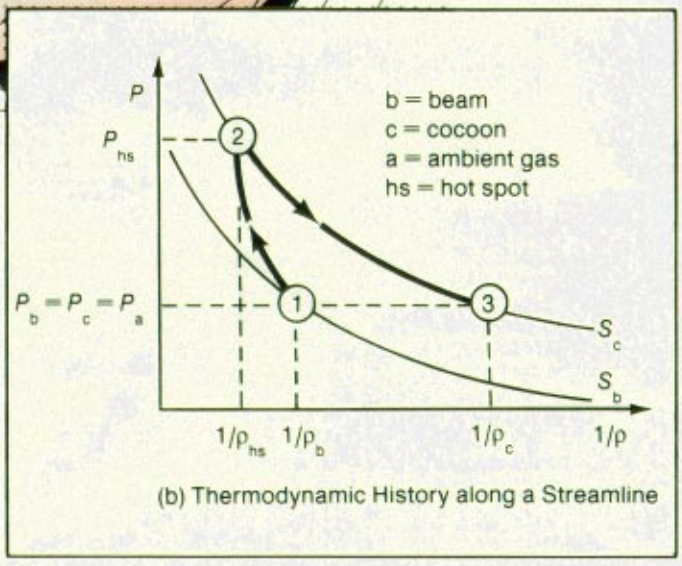

(b) Thermodynamic History along a Streamline

(a)

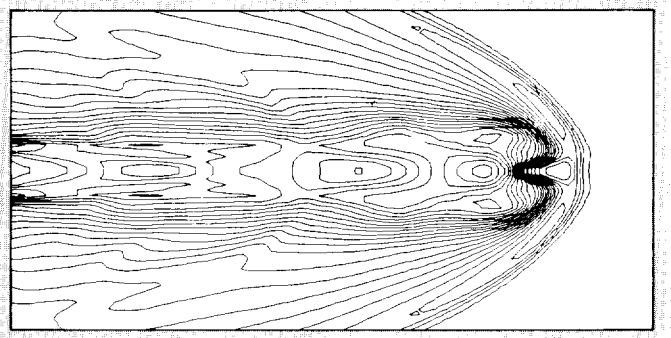

Grid size: one-quarter of the beam radius in both dimensions.
Algorithm: donor-cell advection.

(b)

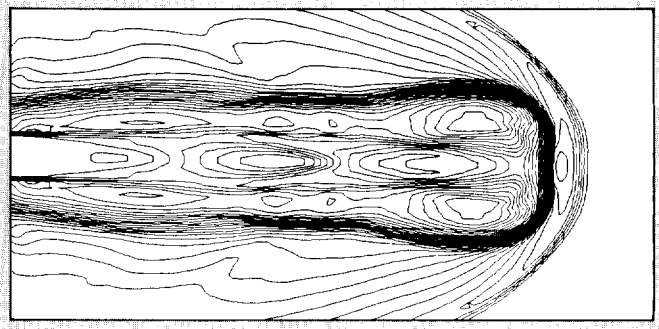

Grid size: one-quarter of the beam radius in both dimensions.
Algorithm: van Leer monotonic advection.

(c)

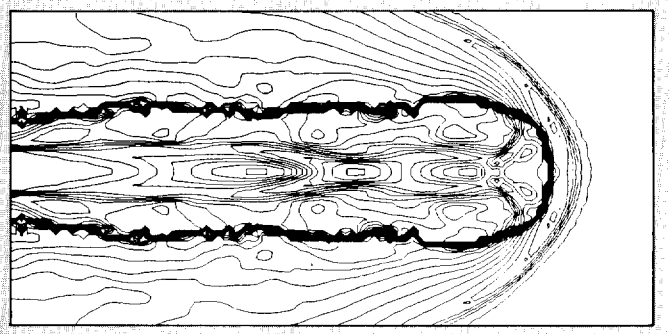

Grid size: one-quarter of the beam radius in both dimensions.
Algorithm: van Leer monotonic advection with a multi-material interface to track the jet boundary.

(d)

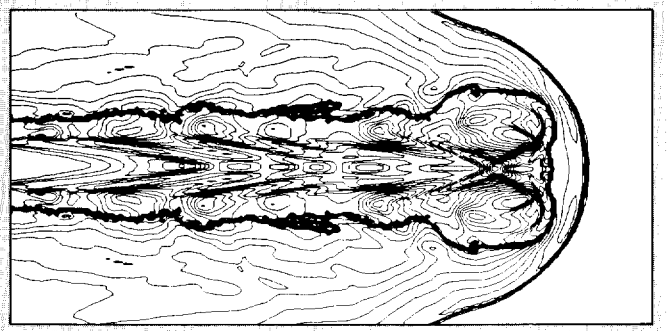

Grid size: one-eighth of the beam radius in both dimensions.
Algorithm: van Leer monotonic advection with a multi-material interface to track the jet boundary.

(e)

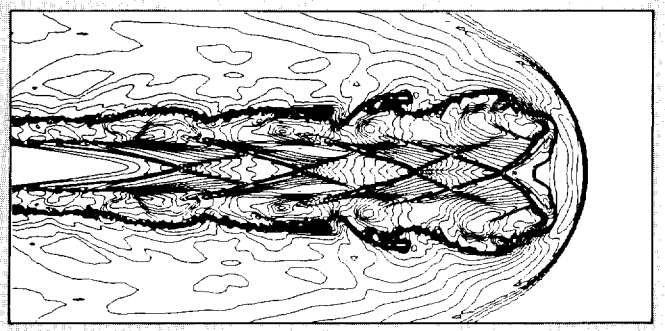

Grid size: one-sixteenth of the beam radius in both dimensions.
Algorithm: van Leer monotonic advection with a multi-material interface to track the jet boundary.

analytic solutions or experimental data exist for comparison? In principle, we cannot be sure; in practice, however, we can verify, through a convergence study, that our simulation captures the important physical structures and processes. Figure 9 displays the results of a convergence study in which we investigated the effects of numerical techniques and grid resolution on the structure of a *(M* = 6,n = 0.1) jet. Scanning the figure from top to bottom, one sees the flow field come into focus as the accuracy and capability of the algorithms are improved and as the grid resolution in each dimension is doubled and then doubled again. Note that all of the key flow features (beam, cocoon, working surface, and embedded shocks) revealed at the high resolution of Fig. 9e also appear in the solution computed at half that resolution, Fig. 9d. The same cannot be said of Fig. 9c.

We used the resolution of Fig. 9d for our simulations but increased the number of zones by a factor of 4 to extend the spatial domain beyond that of Fig. 9. Many extragalactic jets are very long, with length-to-width ratios of up to 100. Our 75-by-640 grid allows us to study jets with lengths of up to 40 jet diameters—well within the range of observed extragalactic jets. Figure 9, as well as the consistency of Fig. 8 with "textbook" supersonic flow structures, gives us confidence that our numerical simulations are producing reliable results.

We have delved into the structural details of a single jet to illustrate the similarities and differences between laboratory jets and our simulations. In the remainder of this article we explore how both jet structure and stability change as the parameters *M* and n are varied.

We did numerical simulations corresponding to thirteen points in the *(M,* n) parameter space. We varied *M* between 1.5 and 12 and n between 0.01 and 10. Jet power, which is proportional to $M^3/\sqrt{\eta}$, varied by roughly four orders of magnitude between the lowest power, *(M*= 1.5, n = 1) jet and the highest power *(M* = 12,n = 0.01) jet. Although jets of even lower density and higher Mach number may be relevant to astrophysics, our survey has revealed the important trends that seem applicable to astrophysical objects. It should be noted that our survey covers a range of parameters that far exceeds what has been investigated in the laboratory. Laboratory jets rarely exceed Mach 3 and are almost exclusively more dense than the ambient gas. As we shall see, the density ratio—a parameter that is seldom varied systematically in laboratory studies—has a profound effect on jet morphology and stability.

Jet Morphology

Figure 10 tells the story of jet morphology in snapshots of our simulated jets arranged according to their values of *M* and n. All the jets are pictured at the same length.

Two general trends are apparent, Scanning the third column from high to low density ratios, we see a marked thickening of the jet. A jet with a low density ratio (n < 1) builds a thick cocoon of backward flowing gas around itself as it propagates, whereas a jet with a high density ratio (n > 1) is just a naked beam, lacking a cocoon altogether. Scanning the third row from low Mach number to high Mach number, we see that the spatial extent of the cocoon increases, At low Mach numbers the cocoon is but a lobe of material at the head of the jet, whereas at high Mach numbers the cocoon surrounds the central supersonic beam along its entire length. The combined effect of these trends is that only jets with low density ratios and high Mach numbers possess extensive cocoons.

These qualitative trends can be understood with the help of a few simple concepts and equations. As mentioned earlier, the cocoon is supplied by gas that flows through the jet head at a rate proportional to $v_b - W$. Equation 1 tells us that this rate is small in high-η jets, since $W \simeq v_b$ for $\eta \gg 1$, and large in low-η jets, since $W \ll v_b$ for $\eta \ll 1$. Thus, on kinematic grounds alone one would expect an inverse correlation between density ratio and the size of the cocoon.

This inverse correlation is enhanced by the shock heating of the jet gas at the terminal shock. The amount of shock heating at the terminal shock is related to M_W^2, where the relative Mach number M_w is defined as $(v_b - W)/cb$. With the help of Eq. 1 and the definition of *M,* we find that $M_w = M/(1 + \sqrt{\eta})$. We can see that for a given *M,* M_W, and thus the amount of shock heating, is largest when n is smallest. The greater the shock heating, the more the gas flowing into the cocoon must expand to match the ambient pressure. Thus, a small n implies not only a large rate of flow into the cocoon but also a greater expansion of the shock-processed gas. The result, in agreement with our simulations, is a cocoon with a relatively large volume and low density.

A similar argument, but now with n held fixed, suggests that larger Mach numbers imply greater shock heating, greater pressure differences between the working surface and

Fig. 9 Effects of resolution (dimensions offinite-difference grid) and algorithmic accuracy on jet structure, as revealed by isodensity contours, for a supersonic jet with initial parameters $M = 6$, $\eta = 0.1$, $K = 1$, and $\theta = 0$. (a) A low-resolution, first-order-accurate computation shows little internal structure of the jet and excessive smearing of the jet boundary. (b) A low-resolution, second-order-accurate computation shows a sharpening of internal structure and boundary. (c) A low-resolution, second-order-accurate computation with interface tracking shows a sharply defined jet boundary but little change in internal structure. (d) A computation with the same algorithms as in (c) but twice the resolution reveals considerable internal structure, including the central supersonic beam, internal shock waves, the cocoon, and waves at the boundary. (e) A computation with the same algorithms as in (c) and (d) but twice the resolution of (d) shows sharply focused internal structure with qualitatively the same features as in (d).

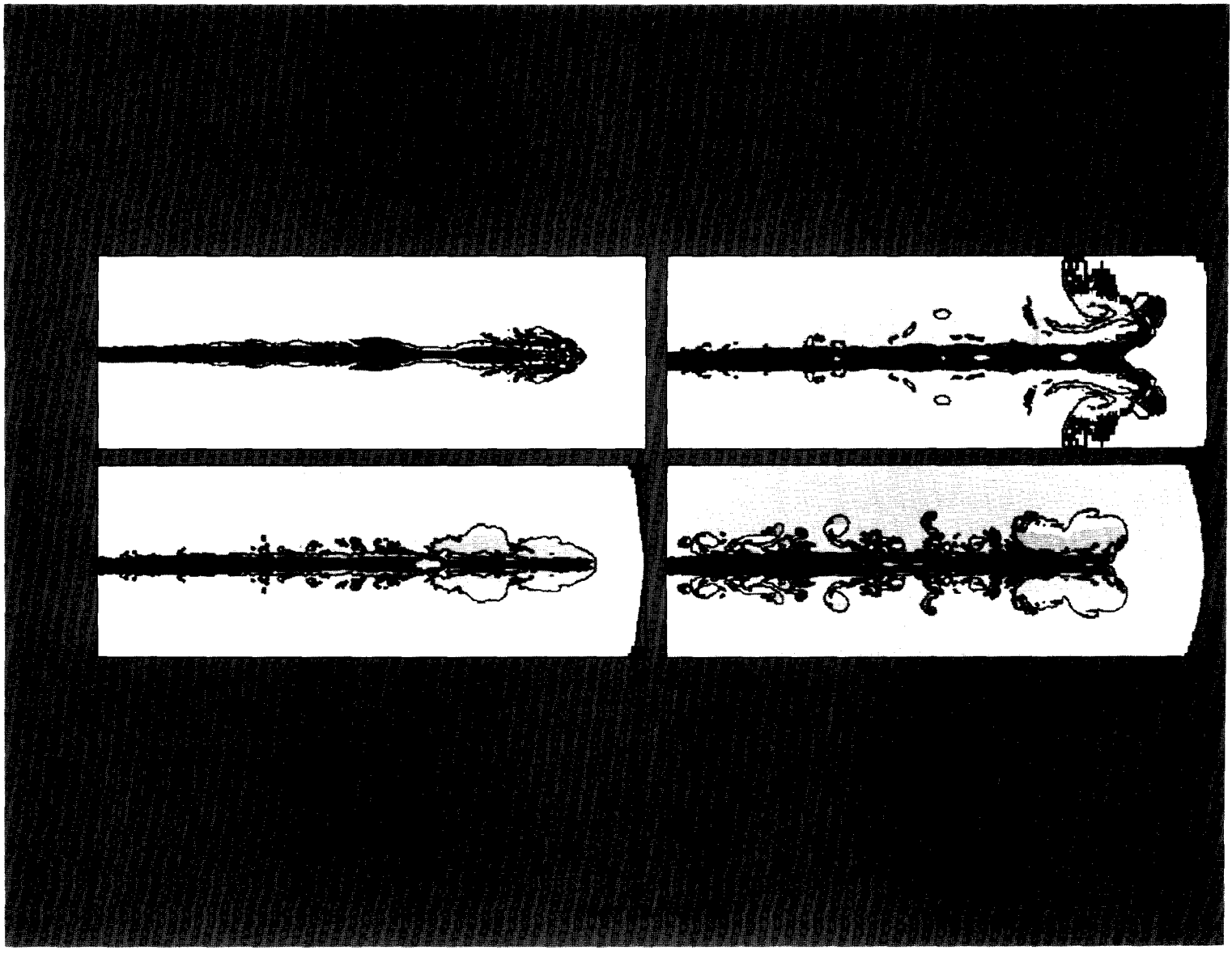

Fig. 10. Dependence of the flow morphology of pressure-matched supersonic jets on the dimensionless parameters M and n. In these kinematic plots the supersonic beam and the bow shock are shown in black, the backward flowing ($v_z < O$) cocoon gas in white, the forward flowing ($v_z > O$) cocoon gas in gray, the undisturbed ambient gas in dark gray, and the disturbed ambient gas in light gray. The simulations reveal an inverse dependence of cocoon thickness on density ratio n and a direct dependence of cocoon length on Mach number M.

the ambient gas, and thus cocoons with larger volumes.

Shear instabilities on the cocoon boundary tend to limit the extent of cocoons for jets with low Mach numbers, The gas in the cocoon generally flows back toward the source, as indicated by the white regions in Figure 10. This backflow is resisted by corrugations in the cocoon boundary, such as are produced by the Kelvin-Helmholtz instability. At low Mach numbers the combined effects of low pressure difference and instability-induced flow resistance serve to localize the cocoon gas to a lobe near the head of the jet.

Can we use these morphological trends to infer the physical conditions in extragalactic radio sources? In principle, yes, but translating from a fluid flow field to a radio surface-brightness distribution is not straightforward. The main uncertainty is the quantitative relationship between synchrotron emissivity and thermal energy in the flow field. In the simplest model one assumes that a small but constant fraction of the thermal energy density is equally divided between the radiating relativistic electrons and the mag-

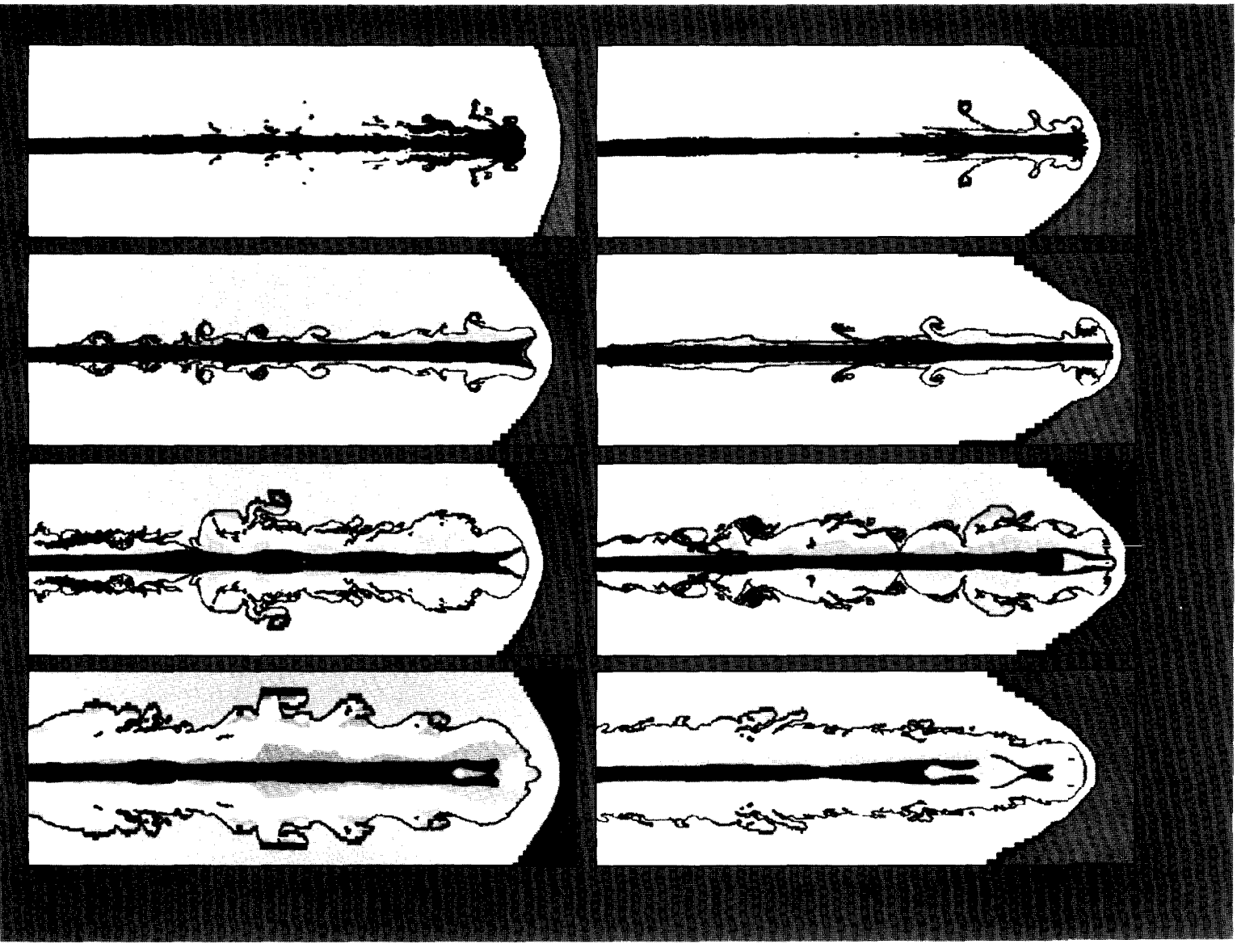

netic field, One then can derive a completely local prescription relating the total synchrotrons emissivity to the thermal pressure. This prescription has the form P^q, where $1.75 \leq q \leq 2$. We have derived hot-spot morphologies by applying this prescription to the working surface and have reproduced many features observed in the hot spots of radio lobes, However, mapping lobes and cocoons will require a more detailed emission model that takes into account the sources and sinks of the energetic electrons, in particular, the radiative and adiabatic expansion losses experienced by a parcel of synchrotron-emitting plasma as it flows from the working surface into the cocoon.

When observed at low frequencies, powerful double radio sources generally exhibit extensive cocoons with mean diameters far in excess of their hot-spot diameters, which we may take as measures of the beam diameters. The morphological trends discussed above imply very large Mach numbers ($M \gg 10$) and very low density ratios ($\eta \ll 0.01$) for these jets. Since the kinetic power of a jet varies as $M^3/\sqrt{\eta}$, jets with the thickest, most extensive cocoons should be the most powerful. in agreement with observation,

Although we understand the trends in morphology on a qualitative level, our attempts to quantify these effects analytically have not been successful Nonlinear and time-dependent effects are just too complicated. For example, the terminal-shock structure is complex and time-dependent, which implies that the cocoon gas is highly inhomogeneous, These inhomogeneitics lead to mass motions (vortices) within the cocoon that perturb the central beam and ultimately contribute to the unsteadiness of the terminal shock. In the face of such complex and coupled effects, numerical simulations arc the best predictive tool we have for the structure of time-dependent jets.

Pinch Instabilities

SIDEBAR 4

and the Bernoulli Effect

Jet Stability

Numerical simulation is also a powerful tool for studying the effects of instabilities in time-dependent jets. This approach complements the traditional analytic tool of linear perturbation theory, which completely characterizes all modes of instability only in the small-amplitude limit. In contrast to linear theory, our simulations show which modes grow to large amplitudes and how they ultimately affect the flow. We now have some tantalizing hints that Kelvin-Helmholtz instabilities. which disrupt laboratory jets with low Mach numbers, may be reduced or totally absent in the high-Mach-number jets emerging from radio galaxies and quasars. In addition, our simulations confirm recent analytic predictions of the existence in supersonic jets of a new family of modes of the Kelvin-Helmholtz instability and characterize for the first time the nonlinear behavior of the new modes. To motivate our discussion. we review the key results gleaned from analytic studies of jet stability,

Linear Stability Theory

A simple analysis of the growth of axisymmetric, or pinch, modes of instability in supersonic beams is given in Sidebar 4, "Pinch Instabilities and the Bernoulli Effect." This analysis predicts that the relation

$$M = 1 + \sqrt{\eta} \qquad (2)$$

defines a stability boundary in the *(M,n)* plane. For $M < 1 + \sqrt{\eta}$, the pinch modes grow, whereas for $M > 1 + \sqrt{\eta}$, they damp. This analysis applies to a purely longitudinal mode, that is, one that introduces no transverse structure within the perturbed channel. Such a mode corresponds to the fundamental axisymmetric mode of instability}.

In 1981 Attilio Ferrari and coworkers in Bologna determined from perturbation theory that a whole family of unstable (that is. capable of growth) higher order modes exists

What happens to a fluid beam when its flow is slightly constricted? Does the flow resist the constriction and remain stable? Or does the constriction grow and pinch off the flow? Here we use a simple argument based on Bernoulli's principle to derive the conditions under which supersonic flow is susceptible to pinch instabilities, or, in other words, is unstable to longitudinal constrictions.

To establish the basic mechanism that drives a pinch instability, we consider first in Fig. Al the steady flow of an incompressible fluid, such as water, in a pipe with a localized constriction. The velocity and pressure of the fluid far from the constriction are v_o and P_o, respectively. At steady state the mass flux, *pvA*, is constant along the length of the pipe, Since the fluid is incompressible (that is, p is constant) the fluid velocity v must increase when the cross-sectional area *A* decreases, The Bernoulli principle states that along a fluid streamline the total specific energy *E* remains constant:

$$E = \frac{1}{2} v^2 + \frac{\gamma}{\gamma - 1} \frac{P}{\rho} = \text{constant} . \qquad (1)$$

Consequently, if p remains constant and *v* increases, the pressure *P* in the vicinity of the constriction must decrease. Figure A2 shows what happens if the channel wall is replaced by a static background fluid of uniform pressure P_o. Since the beam pressure *P* near the constriction is less than the background pressure P_o, the channel boundary will move inward, further constricting the flow. By the above reasoning further constriction leads to even higher velocities, lower pressures. and even further constriction.

Precisely this sequence of events is responsible for pinch instabilities in subsonic jets, In principle, an initial constriction of arbitrarily small amplitude will be amplified by the Bernoulli effect until the constriction completely pinches off the flow. In actuality, the ambient fluid following the channel boundary inward at the point of constriction is swept into the channel and carried downstream by the flow as in Fig. A3. As a result, pinch instabilities contribute to the mixing of a subsonic jet with its environment.

When the beam is supersonic, two other effects come into play. First and most important. the compressibility of the fluid can no longer be ignored. Thus the constancy of the mass flux no longer implies an increase in velocity with a decrease in area. Instead the density increases so rapidly as the area decreases that the velocity decreases also. A general mathematical expression relating velocity change to area change in a flow channel of slowly varying cross section is

$$\frac{dv}{v} = \left(\frac{v^2}{c^2} - 1 \right)^{-1} \frac{dA}{A} , \qquad (2)$$

where c is the speed of sound in the fluid. We see that if the flow is subsonic (v < c), its velocity increases *(dv* > 0) at a constriction *(dA* < 0) just as it does in an incompressible fluid, whereas if the flow is supersonic (v> c), its velocity decreases *(dv* < 0) at a constriction *(dA* < 0).

A naive application of the Bernoulli principle would predict that all supersonic beams are stable to the pinch instability, since by Eqs. 1 and 2 the pressure now *increases* at a constriction and thus resists further pinching. This prediction is incorrect because we have failed to take into account the effects of the motion of the boundary in the direction of the flow. As shown in Fig. B1, the instability created when one fluid moves past

Fig. A. Incompressible Flow

(1) One-Dimensional Flow in a Pipe

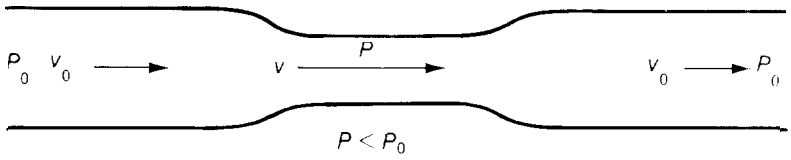

(2) Pinch Instability in Subsonic Flow

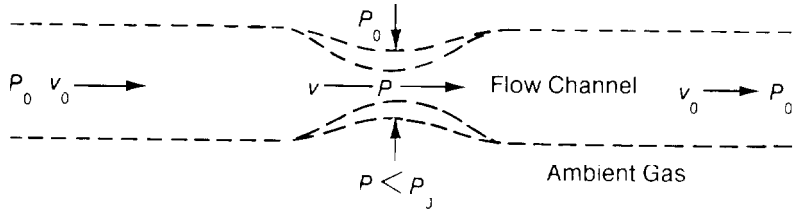

(3) Entrainment of Ambient Medium

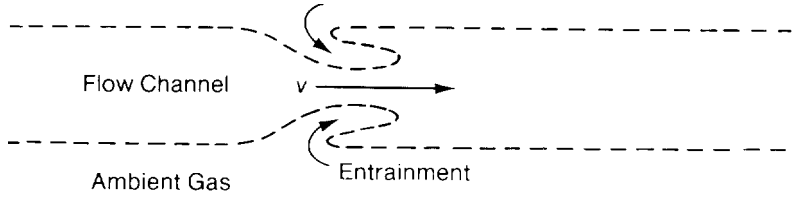

Fig. B. Convective Instability in Compressible Flow

(1) Laboratory Frame

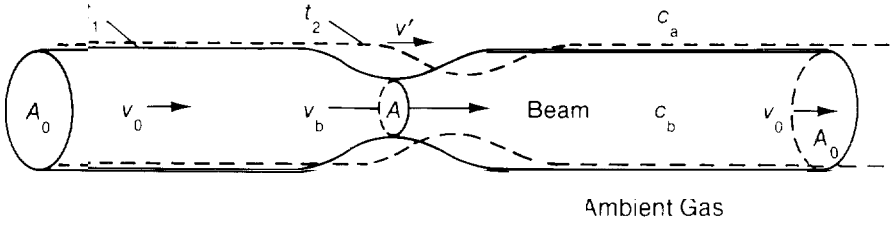

(2) Comoving Frame

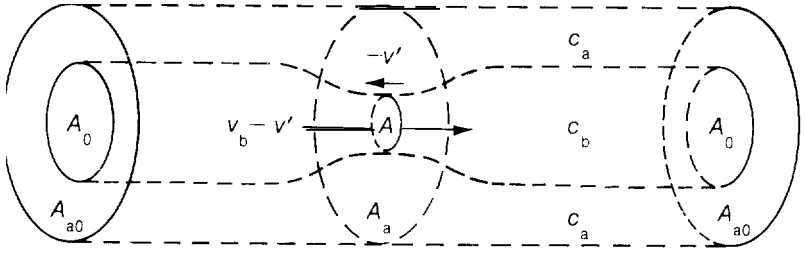

another (the Kelvin Helmholtz instability) is a convective instability; that is, the waveform of the perturbed boundary is carried downstream with some velocity v.

Figure B2 shows the flow in a frame moving at velocity v'. In this frame the beam flows through the constriction with a relative speed of v_b — v', and the ambient gas flows past the constriction with a relative speed of —*v'*. Now consider the Bernoulli effect in the two flow channels shown in Fig. B2—one inside the jet boundary and one surrounding it. To guarantee pinching. we require that at the constriction the pressure decrease inside the jet boundary and increase outside the jet boundary. *This will be the case if both the jet gas and the ambient gas move subsonically with respect to the constriction, since,* from Eqs. 1 and 2, only for relative Mach numbers (ratios of flow velocities in the moving frame to sound speed) less than unity will the channel area and the pressure vary in the same direction. Therefore, a sufficient condition for instability is that v_b - v' < c_b and v' < c_a, where c_b and c_a are the speeds of sound in the beam gas and the ambient gas, respectively. Adding the two inequalities eliminates the unknown v' and yields the condition

$$v_b < c_b + c_a . \qquad (3)$$

Thus, on very simple physical grounds instability requires that the jet speed be subsonic with respect to the sum of the internal and external sound speeds.

To express this condition in terms of the dimensionless parameters Mach number *M* and density ratio n, we eliminate c_a by invoking the pressure balance between the jet and ambient gases ($\rho_a c_a^2 = \rho_b c_b^2$) and obtain

$$M < 1 + \sqrt{\eta} . \qquad (4)$$

This relationship, which was first deduced by David Payne and Haldan Cohn from a dispersion analysis of the linearized equations of motion, thus follows simply from the fact that the growth of pinch instabilities requires subsonic flow of both beam gas and ambient gas relative to the moving constriction. ■

at all Mach numbers greater than unity. These so-called reflection modes derive their name from a special property of a supersonic shear surface, namely, for certain angles of incidence, a sound wave will be amplified upon reflection from the surface. A reflection mode instability in a supersonic beam follows from the repeated amplification of perturbations reflected back and forth between the channel walls. A recent analysis of the reflection modes by David Payne and Haldan Cohn has shown that at the resonant wavelength of each mode, the wave fronts of the perturbation meet the beam boundary at the Mach angle. Thus, the reflection modes are largely transverse in character, in contrast to the fundamental mode. Figure 11 shows the structure, as computed by Payne and Cohn with linear theory, of the fundamental pinch instability and of the first and second reflection pinch instabilities.

A key finding of Payne and Cohn is that Eq. 2 defines a *transition* boundary (Fig, 12) in the dominant mode of instability: for $M < 1 + \sqrt{\eta}$, reflection modes are absent and only the fundamental mode exists, in agreement with our naive analysis; for $M > 1 + \sqrt{\eta}$, the reflection modes dominate. This boundary is indicated in Fig. 12 by the upper dashed line. Note that the majority of our simulated jets (solid circles) reside in the reflection-mode regime; in particular, five cases straddle the transition boundary. We can therefore investigate whether indeed a transition in the modal character of nonlinear pinch instabilities occurs, and if so, what effect the transition has on jet propagation.

Instability in the Nonlinear Regime

How do wc detect an instability in a numerical simulation'! Figure 13 illustrates the growth of a reflection-mode instability in the $(M = 3, \eta = 0.1)$ jet discussed in detail above. Figure 13a is a color-coded plot of gas pressure for this jet at the same instant in its evolution as that depicted in Fig. 7. The continuity of color at the orifice indicates that we arc indeed fulfilling our pressure-

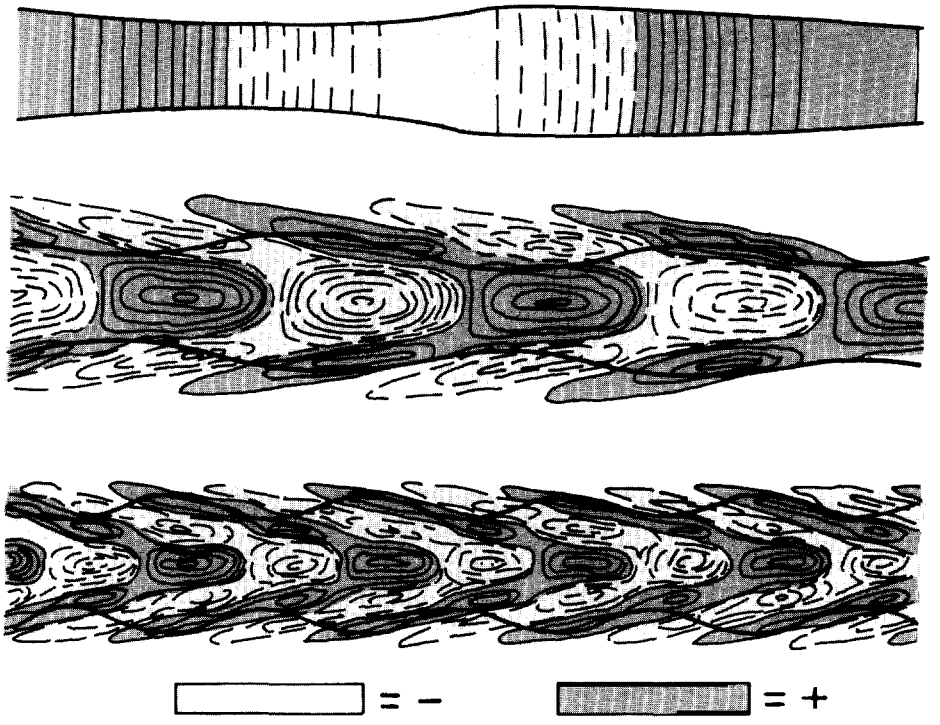

Fig. 11. Structure of the fundamental and first and second reflection pinch instabilities in a (M= 5,n = 0.1) supersonic beam as predicted by linear perturbation theory. Dark and light shades of gray correspond to regions of positive and negative pressure about the mean. Whereas the fundamental pinch mode is purely longitudinal, the nth reflection mode possesses n nulls in the radial perturbation function. Adapted from David G. Payne and HaIdan Cohn, **Astrophysical Journal** ***291(1985):655-667.***

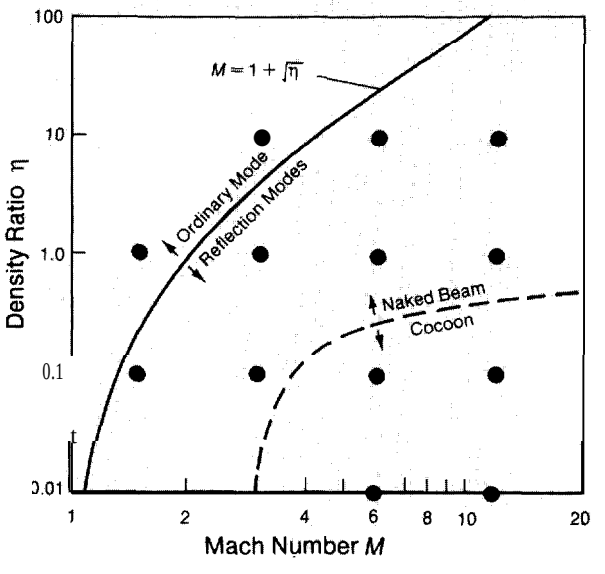

Fig. 12. Transition boundaries in (M, n) parameter space. The transition boundary separating the regions of dominance of the ordinary mode ($M < 1 + \sqrt{\eta}$) and of the reflection modes ($M > 1 + \sqrt{\eta}$) of the Kelvin-Helmholtz pinch instability was analytically determined (see Sidebar 4). The approximate location of the line of demarcation between jets with cocoons and those without cocoons (naked beams) was determined from a visual inspection of the jets displayed in Fig. 10. The solid circles indicate the initial (M, n) values for those jets.

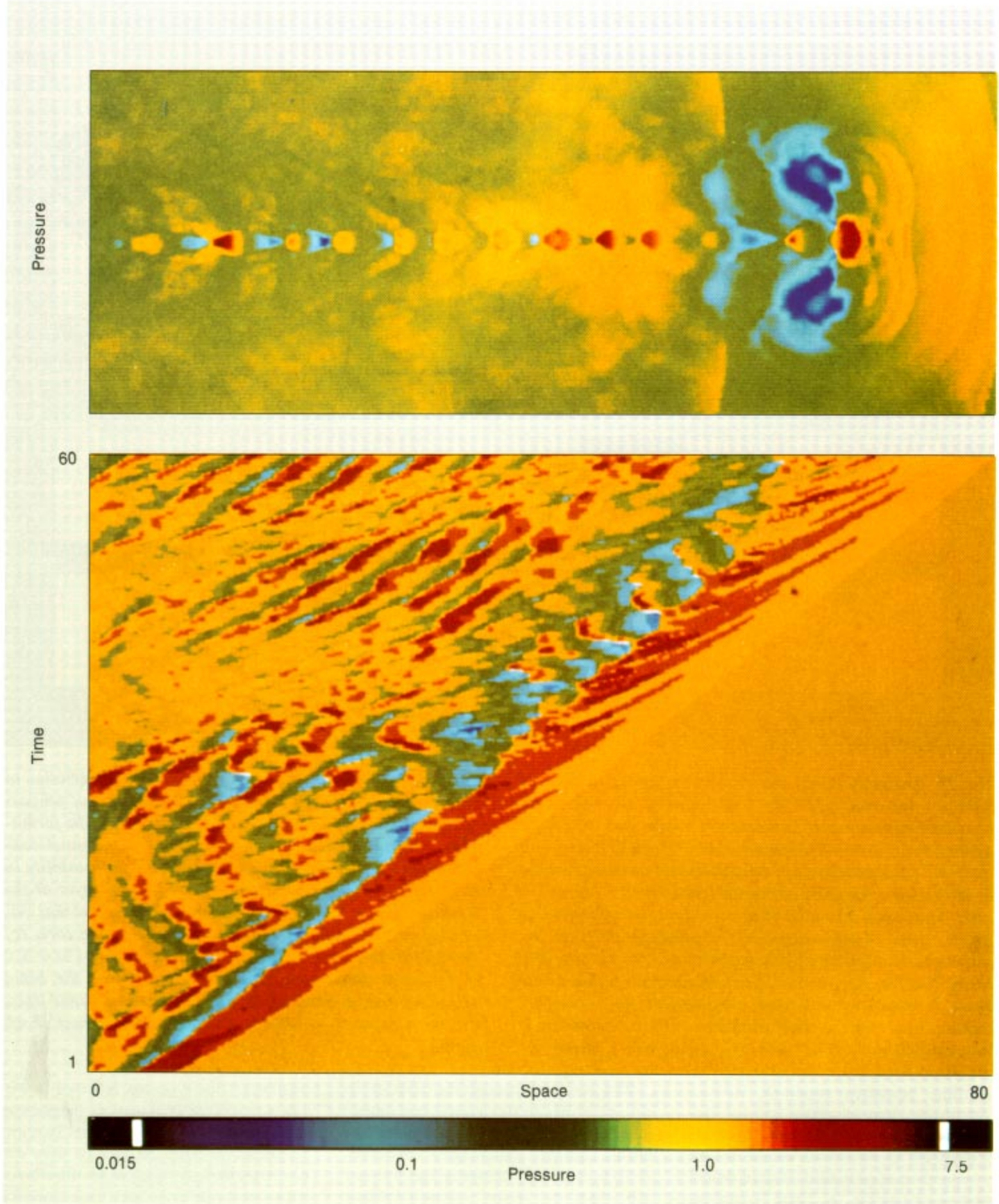

Fig. 13. Pressure fluctuations in the ($M = 3, \eta = 0.1$) supersonic jet of Figs. 4 and 7 caused by the nonlinear growth of a reflection-mode pinch instability. Pressure values vary according to the color code. (a) The spatial pressure distribution at $t = 60$ shows the high-pressure knots and terminal "hot spot" produced by the embedded shock waves displayed in Fig. 7c. (b) The space-time distribution of axial pressure shows the advance of the bow shock into the constant-pressure ambient gas and the emergence and subsequent motion of the knots (red diagonal ridges).

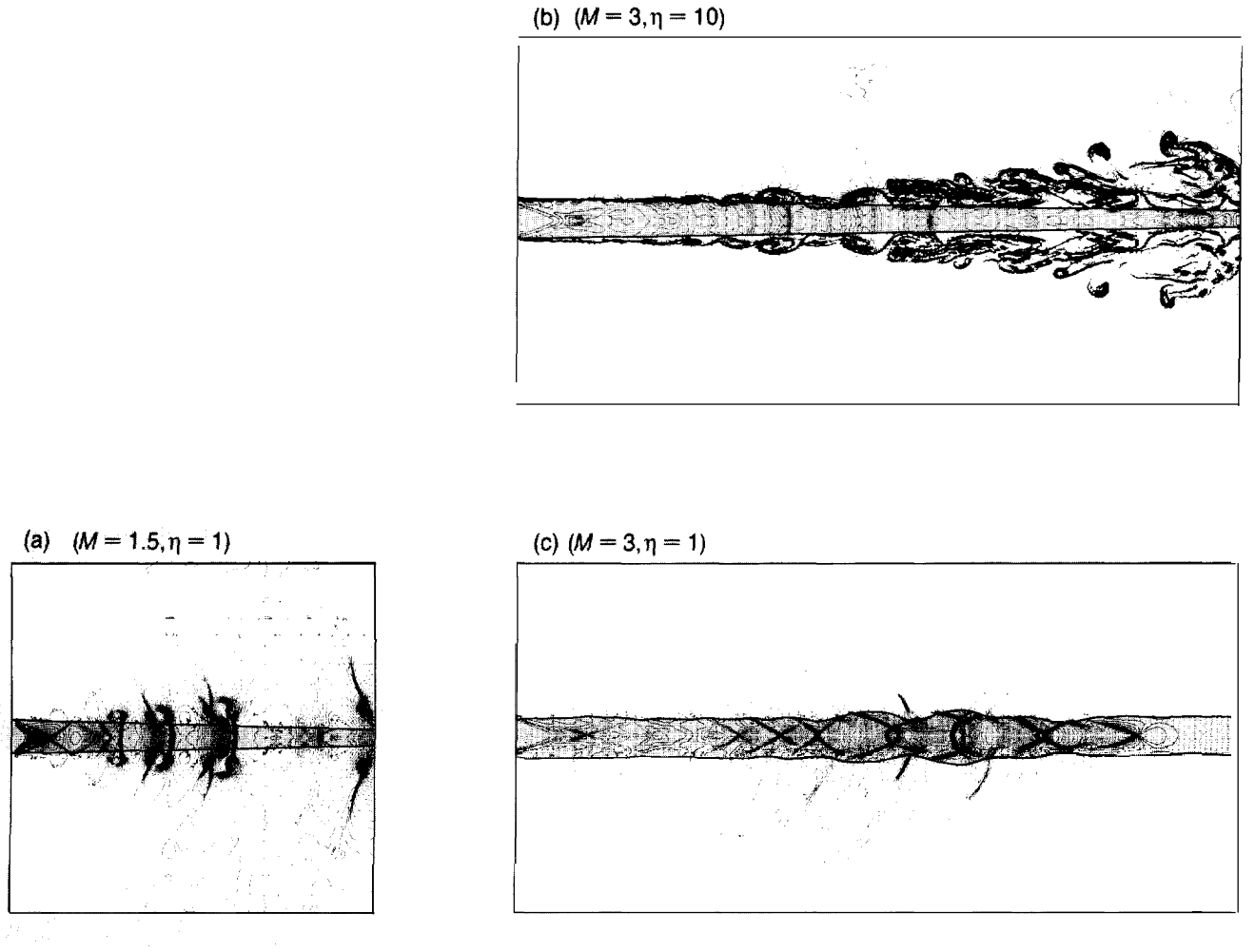

Fig. 14. High-resolution simulations in the nonlinear regime for supersonic jets on both sides of the transition boundary between the fundamental mode and reflection modes of the Kelvin-Helmholtz pinch instability. At t = 0 the beam extends across the computational domain, flowing in at the left with fixed parameters and flowing out at the right. The initial jet radius is resolved into twenty computational zones. A perturbation is applied at the inlet by continuously admitting beam gas with a l-percent pressure excess (that is, K = 1.01). The subsequent evolution of the beam is computed by using a numerical fluid-interface technique to track the beam boundary until the instability is well established. (a) Growth of a fundamental pinch instability in a (M= 1.5, n = 1) beam leads to constriction of the beam boundary (dark line) and entrainment of tongues of ambient gas. Isopressure contour lines reveal the formation of normal shock fronts upstream of the channel constriations. (b) Growth of a fundamental pinch instability in a (M = 3, n = 10) beam establishes a mixing layer at the beam boundary. The isodensity contour lines reveal that this mixing layer rapidly spreads into the supersonic core. (c) Growth of the first reflection pinch instability in a (M = 3, n = 1) beam causes only a mild undulation of the beam boundary and, as revealed by the isopressure contour lines, excites a network of oblique internal and external shock waves.

matching boundary condition *(K = 1).* Nevertheless, large-amplitude pressure fluctuations appear within a few beam diameters downstream of the orifice, caused by the presence there of embedded rarefactions and shock waves (see Fig. 7a). These fluctuations are not tied to the orifice, in marked contrast to the pressure fluctuations in laboratory supersonic jets, which are excited with large amplitudes at the nozzle by the pressure mismatch there and subsequently decay downstream,

We can now understand the origin of the network of oblique shock waves that appears in the beam in Fig. 7a—it is the result of the oblique acoustic disturbances (reflection-mode instabilities) pictured in Figs. 11b and 11c, which have grown to finite amplitude and steepened into shock fronts. The superficial resemblance of the resulting shock network to the diamond-shaped steady-state shock pattern displayed in Sidebar 3 breaks down when wc investigate the time evolution of nonlinear reflection-mode instabilities. This evolution is traced in Fig, 13b, a plot of the axial pressure distribution within the jet as a function of time. *To* orient the reader. we point out that the color discontinuity along the diagonal line from lower left to upper right is the space-time trajectory of the bow shock as it is driven into the ambient gas (which has uniform pressure) by the advance of the jet head. The sharp jump from blue and green to orange and red traces the motion of the terminal shock front. The red diagonal ridges trace the movement of

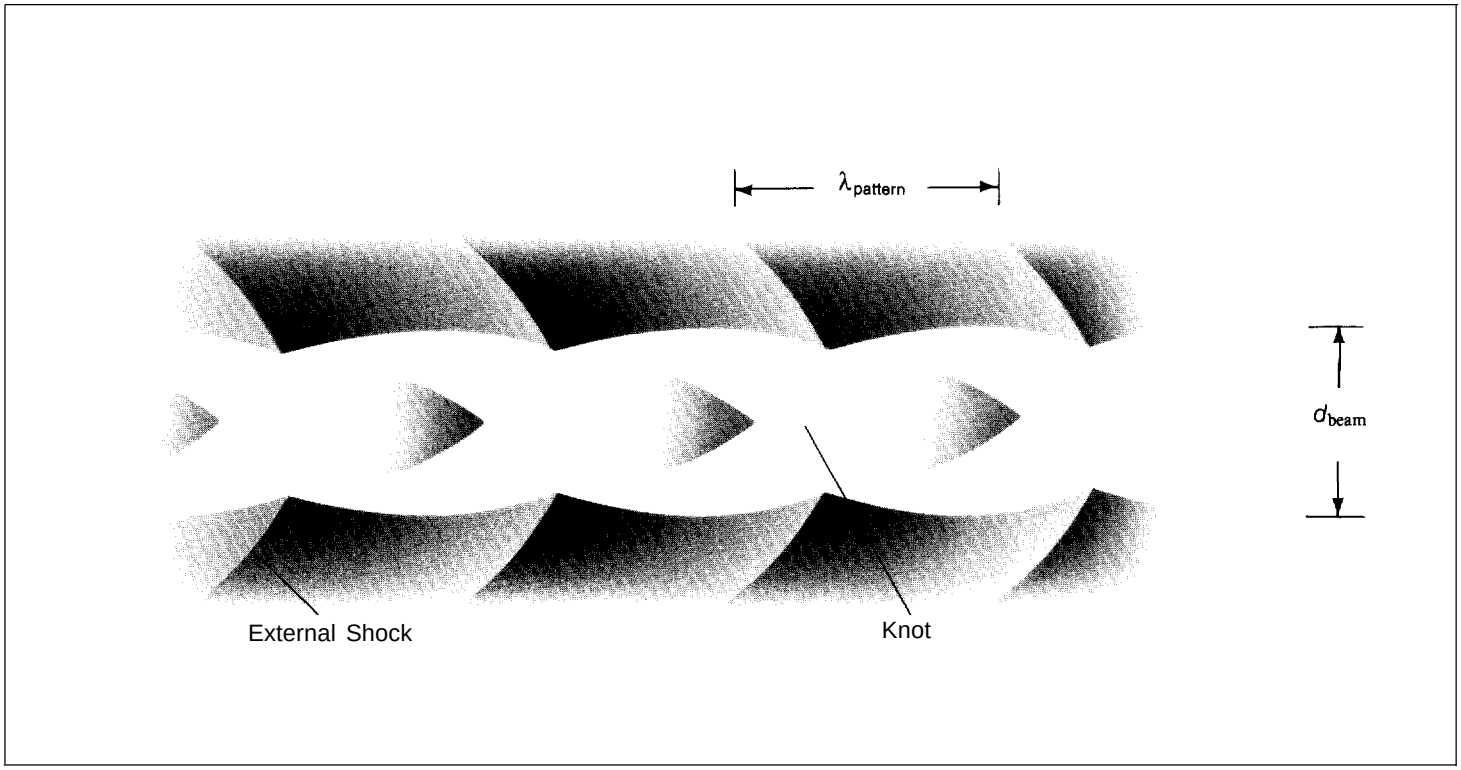

Fig. 15. The shock-wave structure of a nonlinear reflection-mode pinch instability and the resulting temperature distribution. Temperature values are depicted according to an arbitrary scale in which hot is white and cold is dark gray. The pattern created by the saturated oscillation has a wavelength of about 2.5 beam diameters and travels downstream at a speed v_{knot} that is a significant fraction of the beam speed.

the high-pressure knots produced by the embedded shock network and reveal a remarkably well-ordered space-time flow. This pattern indicates that the reflection mode is a convective instability, that is. one that grows in amplitude as the perturbation is convected downstream.

Payne and Cohn suggest that the stationary shock diamonds and high-pressure knots arising in underexpanded ($K > 1$) supersonic jets are a signature of the reflection mode at marginal stability, that is, at a state of zero growth rate and zero phase velocity. Zero growth implies zero damping, and this may well account for the remarkable longevity of the oscillations observed in the plumes of some rocket engines (see Fig. l). Of course, the irreversible processes of shock heating and turbulence do introduce some damping, and the growth of the turbulent mixing layer at the jet boundary ultimately overcomes the oscillations, as shown in Fig. D of Sidebar 3.

An ever-broadening mixing layer is conspicuously absent in Fig. 7a; the clumps of material above and below the beam are what is left of the cocoon as it mixes with the ambient gas (see Fig. 4). In addition, the nearly constant thickness of the green vortex layer in Fig. 7b shows very little spreading of the beam boundary. Reflection-mode instabilities thus seem to be far less disruptive than the fundamental-mode instability.

To further investigate this interesting result, we performed high-resolution simulations of supersonic beams with parameters on both sides of the transition boundary. The results of these calculations (Fig. 14) support the general conclusion that boundary mixing is greatly reduced in supersonic beams satisfying $M > 1 + \sqrt{\eta}$. A more extensive numerical study of the transition from fundamental mode to reflection mode is in progress.

The key features of the saturated reflection mode are summarized in Fig. 15. The mild undulation of the jet boundary is coupled to the network of oblique internal shock waves. Two subtle but important differences between this wave pattern and the steady-state jet depicted in Fig. A of Sidebar 3 arc (1) the reflection of shocks from the boundary as shocks rather than rarefactions and (2) the transmission of a shock into the gas external to the beam. The external shock wave is the mechanism by which the energy of relative motion amplifies the internal reflected shock. Since there is no relative motion between ambient gas and boundary corrugations in underexpanded supersonic jets, no external shock wave is excited in such jets,

We observe the growth of nonlinear reflection modes in all but one of the jets lying within the parameter space below the instability transition boundary and above the boundary for cocoon formation (lower dashed line in Fig. 12). In the one exception, a (M= 1.5,n = 0.1) jet, the shock waves were too weak to be detected numerically. Since the pattern wavelength of the saturated oscillation is about 2.5 beam diameters in the Mach 3 and Mach 6 jets and only slightly greater at Mach 12, the dependence of wavelength on Mach number is quite weak. This result is consistent with perturbation theory, which predicts a maximum growth rate at wavelengths near the beam circumference. The speed of advance of the patterns varies between 10 and 50 percent of the beam speed and is consistent with the density-ratio scaling given in Eq. 1. This is not surprising because ram-pressure balance in a frame comoving with the oblique shocks determines the advance speed of the patterns, just as it determines the advance speed of the working surface. Quite generally, therefore, the high-pressure knots advance with approximately the same speed as the jet head, as can be seen in Fig, 13b.

In principle, cocoon-shrouded beams are also subject to reflection-mode instabilities, We find, however, that cocoon dynamics puts its own imprint on the internal structure of the beam. At high Mach numbers the backflow within the cocoon is also supersonic, and components of this momentum flux normal to the beam drive oblique shock

waves into the beam (Fig. 16). The perturbations are associated with toroidal vortices within the cocoon that drift back toward the source, The oblique shocks they excite possess a less regular pattern than shocks induced by reflection-mode instabilities, and consequently the high-pressure knots are also less regular,

Astrophysical Implications

Knots of enhanced emission, frequently regularly spaced, are observed in numerous extragalactic radio jets (Fig. 17). The nonlinear reflection-mode instability is an attractive candidate mechanism for producing these knots because of our finding that this instability is ubiquitous in highly supersonic jets. The high-pressure knots created by the instability would appear as regions of enhanced emission because of the P^2 scaling of the synchrotrons emissivity mentioned previously.

A prediction of our model is motion of the emission knots. In principle, a measurement of their apparent motion with respect to the galactic nucleus could be used to infer the jet speed and density ratio. Unfortunately, the time scales associated with the evolution of kiloparsec-scale radio jets are too great for this motion to be detectable. Some parsec-scale extragalactic jets and stellar jets also exhibit regular strings of emission knots, and the motion of these knots is detectable with current radio and optical telescopes, Future high-resolution observations of stellar jets with the Hubble Space Telescope and of compact radio jets with the the Very Large Array of radio telescopes can put our model to the test.

Returning to the large-scale radio jets and their remarkable ability to propagate without disruption over intergalactic distances, we propose that the strings of emission knots may be a signature of nature's way out of the stability problem. This may sound contradictory, since the reflection modes that produce the knots are a kind of instability. However, like many other instabilities in

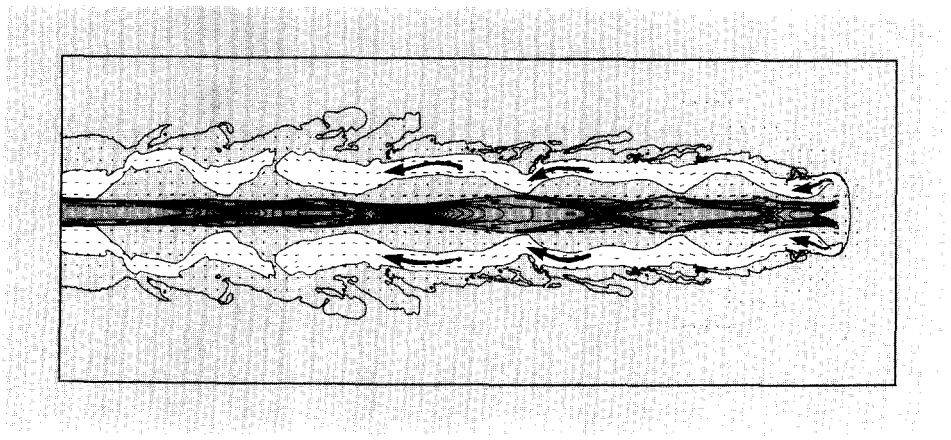

Fig. 16. Interaction of backward flowing cocoon gas (white) with forward flowing supersonic beam gas produces oblique internal shock waves in a ($M = 12$, $\eta = 0.01$) jet. Isocontours of the axial kinetic energy flux $\frac{1}{2}\rho v^3$ are plotted within the jet boundary (heavy line).

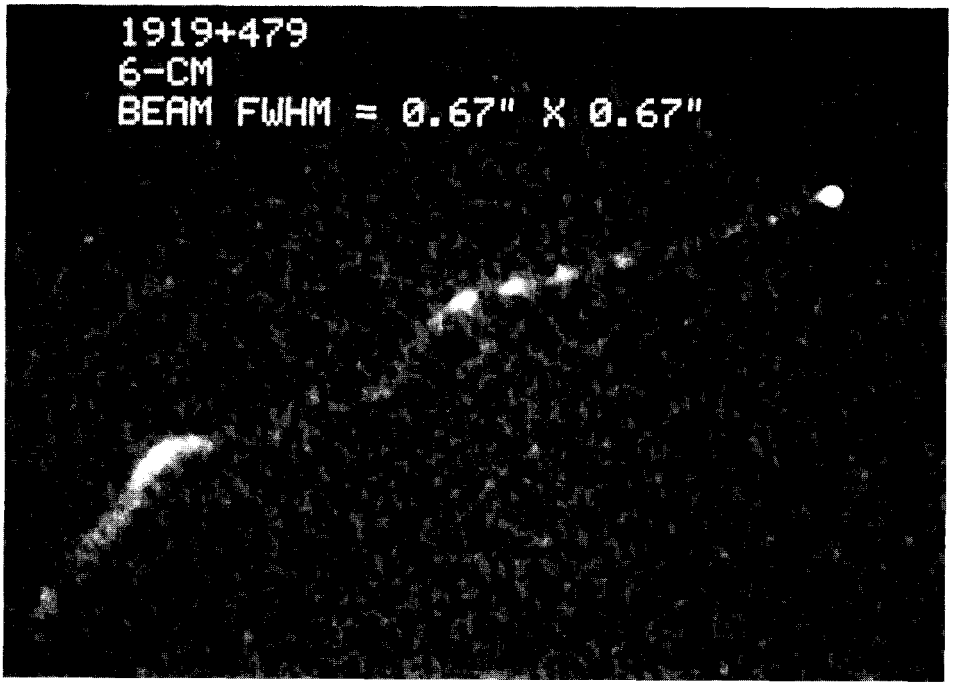

Fig, 17. Radio emission knots in the extragalactic jet 1919+479. Regions of high radio brightness are shown in white. The bright spot to the upper right is the unresolved radio "core" (the source of the jet), which coincides with the nucleus of a giant elliptical galaxy. The onset of large-scale bends in the jet signals its incipient disruption. The radio jet is roughly 300,000 light-years long. (Unpublished VLA image courtesy of J. O. Burns.)

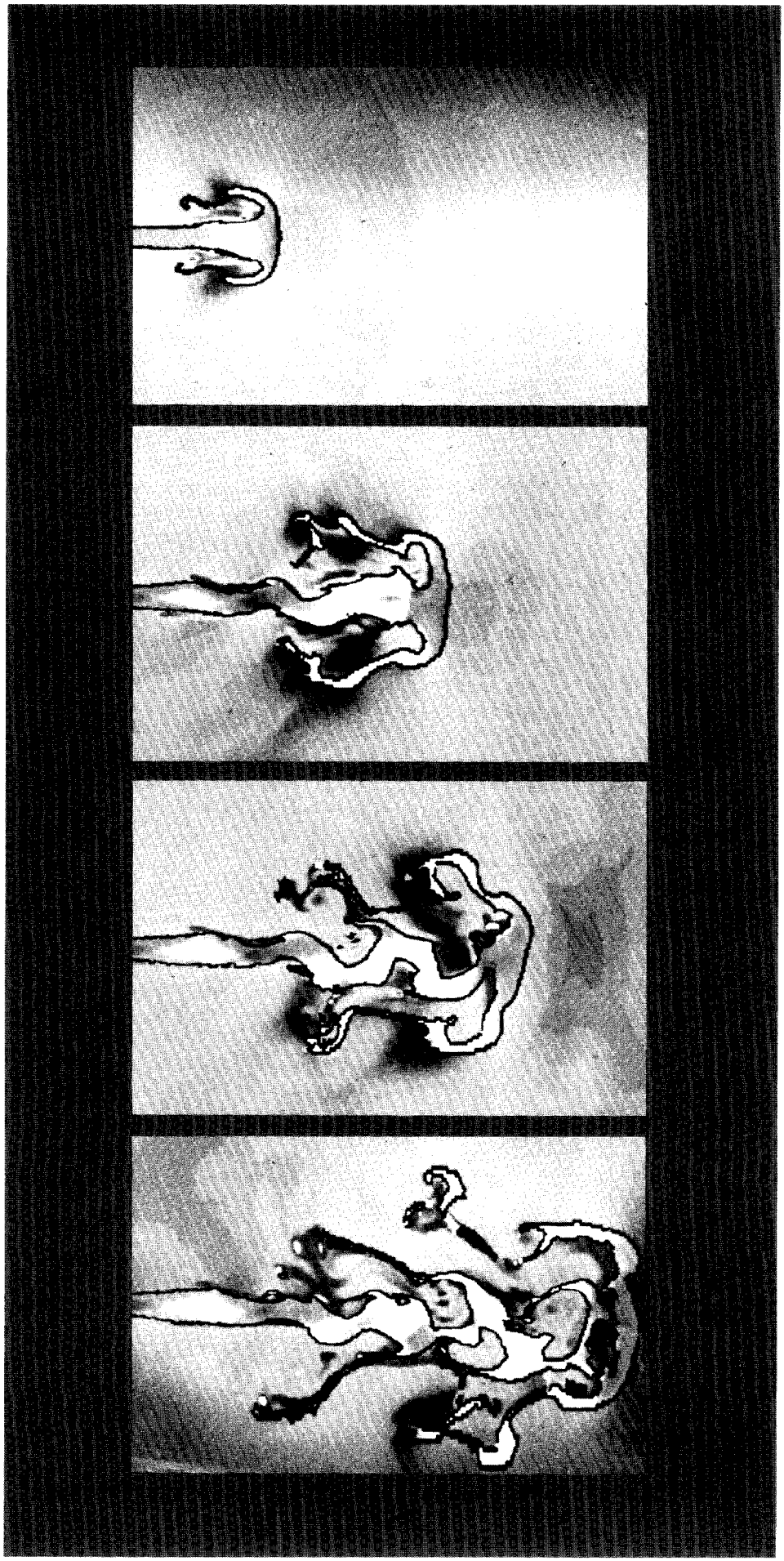

fluids and plasmas, the reflection modes appear to saturate at finite amplitudes and do minimum damage to the flow.

The enhanced boundary stability of the reflection modes is almost certainly exaggerated by our two-dimensional simulations. It is nevertheless known experimentally, but not understood, that the spreading rate of supersonic shear layers drops precipitously beyond Mach numbers of about 5. Another important feature of reflection modes is the existence of oblique internal shock waves. Their oblique character allows the postshock axial flow speed to remain supersonic even though the component normal to the shock is subsonic, These two effects-enhanced boundary stability and minimal flow deceleration—make the reflection mode a benign instability in terms of jet disruption.

In very long jets these small effects may add up to a big effect and ultimately disrupt the flow. Quite often the signature of incipient disruption is the onset of large-scale wiggles in the jet, as can be seen in Fig. 17. This kind of behavior, which is observed experimentally in fluid jets and magnetically confined plasma columns, is a consequence of the growth of nonaxisymmetric instabilities to amplitudes at which nonlinear effects become important. These so-called garden-hose instabilities are fundamentally three-dimensional in character and therefore cannot be studied within the context of two-dimensional axisymmetric numerical simulations. However, two-dimensional

Fig. 18. Numerical simulation of the growth of a kink instability in a two-dimensional "slab'' jet with M = 3 and n = 10. The variable plotted is density. The instability is excited at the inlet by imposing on the beam a sinusoidally varying transverse velocity with an amplitude equal to 5 percent of the beam's axial velocity. The frequency of the perturbation corresponds to the most unstable wavelength: $\lambda = 2d\sqrt{M^2 - 1}$. ***The jet diameter d is divided uniformly into forty zones.***

simulations of a planar "slab" jet do allow us to study the effects of kinking on the flow.

We performed such a simulation for a slab jet with parameters in the ordinary-mode regime, namely $M = 3$ and $n = 10$. As shown in Fig. 18, the amplitude of the oscillations grows rapidly, thereby destroying the directionality of the flow. A similar calculation for a slab jet with values of M and n in the reflection-mode regime also shows growth of kinks, but the kinks grow much more slowly and are of longer wavelength. As we might expect, oblique internal shock waves accompany the bends. These shocks become quite strong as the bend angle becomes large and produce high-pressure knots at the bend. This is a likely explanation for the origin of the bright emission knot at the bend in the radio jet shown in Fig. 17.

Both the axisymmetric and nonaxisymmetric instabilities derive from the interaction between a moving fluid stream and a confining medium. Although the pressure of the intergalactic gas appears adequate to confine the vast majority of radio jets, evidence is accumulating that the jets emerging from distant quasars are too highly pressurized to be confined by their local environment. Magnetic confinement, which is often invoked to explain these observations, would require that the jets carry substantial currents. As we have no unambiguous evidence for the presence or absence of such currents in radio jets, magnetic confinement remains just a hypothesis. It is curious and perhaps significant that Payne and Cohn find that the properties of the linear reflection modes are quite insensitive to the confinement mechanism, be it pressure or magnetic forces. If this finding holds also in the nonlinear regime, strings of emission knots may well be a universal signature of confined supersonic jets.

Outlook

In this article, and in our research, we have emphasized the phenomenology of a set of basic physical laws operating in an astrophysical context and the dependence of this phenomenology on the underlying parameters in order to uncover trends in morphology and stability that may aid in the interpretation of extragalactic radio sources. Far from being detailed source models, our numerical simulations are rather thought-experiments carried out by a computer that show us the consequences of self-consistency in a nonlinear, multidimensional, time-dependent context. An important outcome of our investigation is the discovery of large-scale coherent structures associated with the supersonic beam, the working surface, and the cocoon and of the essential role these structures play in contributing to the phenomenological trends.

We foresee future research in the physics of extragalactic jets proceeding along two complementary tracks: 1) further phenomenological studies aimed at systematically investigating the new dynamical effects that arise when magnetic forces, bulk relativistic motion, and turbulence are incorporated into two- and three-dimensional models, as well as understanding the impact of inhomogeneities, pressure stratifications, and crosswinds in the intergalactic environment; and 2) the development of detailed source models aimed at bridging the gap between simulation and observation by incorporating self-consistent synchrotrons emission models into the dynamical calculations and followed by mapping of the resultant flow field for observable quantities such as the distribution of radio brightness, degree of polarization, spectral index, and magnetic field orientation. Only through such a twin-track approach will we be able to select between competing hypotheses concerning the composition, internal processes, state of motion, and ultimately the origin of extragalactic radio sources and their associated jets, which have fascinated and continue to fascinate twentieth-century astronomers and astrophysicists. The increase in resolving power of our respective tools—radio telescopes and computers—is continuing, if not accelerating, and promises exciting research on into the twenty-first century and progress toward understanding these spectacular cosmic eruptions. ■

Further Reading

R. Courant and K. O, Friedrichs. *Supersonic Flow and Shock Waves. New* York: Interscience Publishers, Inc., 1948.

H. Reichenbach. "Contributions of Ernst Mach to Fluid Mechanics." *Annual Review of Fluid Mechanics* 15(1983):1-28.

R. Ladenburg, C. C. Van Voorhis, and J. Winckler, "Interterometric Studies of Faster Than Sound Phenomena. Part II. Analysis of Supersonic Air Jets." *Physical Review* 76(1949):662-677.

R. D. Blandford and M, J. Rees. "A 'Twin-Exhaust' Model for Double Radio Sources." *Monthly Notices of the Royal Astronomical Society* 169(1974):395-415.

Roger D, Blandford, Mitchell C. Begelman, and Martin J. Rees. "Cosmic Jets." *Scientific American,* May *1982,* pp. 124-142.

Norman J. Zabusky, "Computational Synergetic." *Physics Today,* July 1984.

Michael L. Norman, Larry Smarr, Karl-Heinz A. Winkler, and Michael D. Smith. "Structure and Dynamics of Supersonic Jets." *Astronomy and Astrophysics* 113(1982):285-302.

Larry L. Smarr, Michael L. Norman, and Karl-Heinz A. Winkler. "Shocks, Interfaces, and Patterns in Supersonic Jets." In *Fronts, Interfaces, and Patterns—Proceedings of the Third Annual Conference of the Center for Nonlinear Studies, Los Alamos National Laboratory, Los Alamos, New Mexico, May 2-6, 1983*. Edited by Alan R. Bishop, Laurence J. Campbell, and Paul J. Channell. *Physica* 12D(1984):83-106.

Michael L. Norman, Larry Smarr, and Karl-Heinz A. Winkler. "Fluid Dynamical Mechanisms for Knots in Astrophysical Jets." In *Numerical Astrophysics.* Edited by J. Centrella, J. LeBlanc, and R. Bowers. Portola Valley, California: Jones and Bartlett, 1985.

Michael L. Norman, Karl-Heinz A. Winkler, and L. Smarr. "Knot Production and Jet Disruption via Nonlinear Kelvin-Helmholtz Pinch Instabilities." In *Physics of Energy Transport in Extragalactic Radio Sources—Proceedings of NRAO Workshop No. 9, Green Bank, West Virginia, August 1984,* pp. 150-167. Edited by Alan H. Bridle and Jean A. Eilek. Green Bank, West Virginia: National Radio Astronomy Observatory, 1985.

David G. Payne and Haldan Cohn. "The Stability of Confined Radio Jets: The Role of Reflection Modes." *Astrophysical Journal* 291 (1985):655-667.

Michael L. Norman joined the Laboratory in 1984 as a staff member in the Advanced Concepts and Plasma Applications Group of the Applied Theoretical Physics Division. He received his B.S. in astronomy from the California Institute of Technology in 1975 and his M.S. in 1976 and Ph.D. in 1980 in engineering and applied sciences from the University of California, Davis. While earning his Ph. D., he performed numerical calculations of protostar formation. From 1980 until he joined the Laboratory in 1984 he was a staff member at the Max Planck Institut fur Physik und Astrophysik in Munich where he did the work described in this article. Mike is also an Adjunct Assistant Professor in the Physics and Astronomy Department of the University of New Mexico and is directing the research of a number of graduate students on extragalactic jets.

Karl-Heinz A. Winkler earned his Dr. rer. nat. in physics from the Georg-August Universitat Gottingen in 1976. He then became a staff member at the Max Planck Institut fur Physik und Astrophysik in Munich until August 1984, where he did research on radiation hydrodynamics, star formation, and supersonic jets. In 1978 he became a consultant to Los Alamos and Livermore. Karl-Heinz joined the Laboratory as a staff member in the Applied Theoretical Physics Division during the summer of 1984. He is designing numerical methods and applying them to interesting problems in physics and astrophysics.